The Application of Drone Thermography in Halos, Greece

Scholte, Mason

The Application of Drone Thermography in Halos, Greece

Mason Scholte

BA Thesis 2021
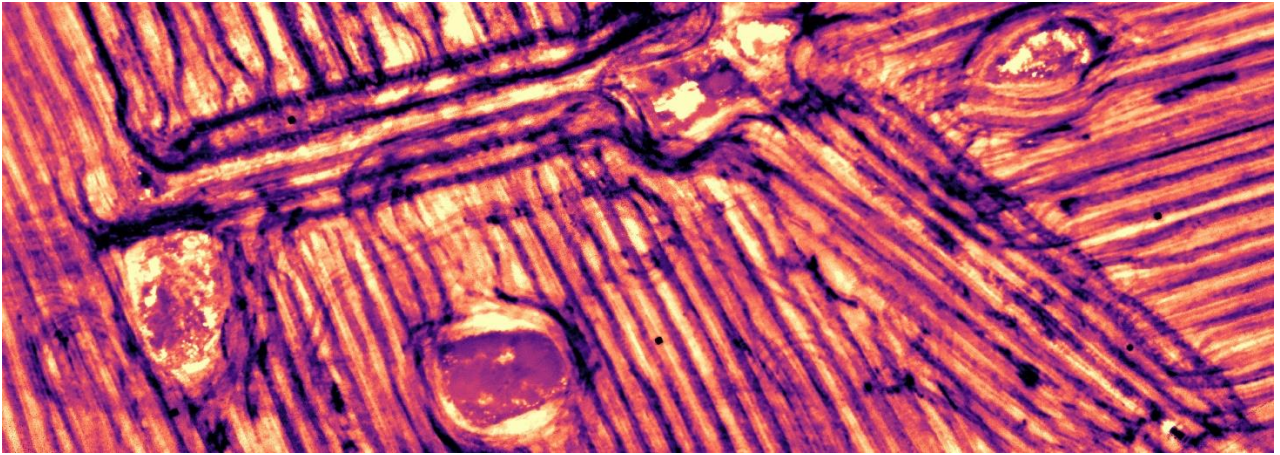
Cover figure: a detail of a thermogram recorded at 21:24 on the 10th of July 2019, showing several tumuli on site C (own work).

Title: The Application of Drone Thermography in Halos, Greece

Author: Mason Scholte s2335239

Course: Thesis BA3, 1083VBTHEY

Supervisor: Dr. K. Lambers

Specialisation: Digital Archaeology

University of Leiden, Faculty of Archaeology

Alkmaar, 15-06-2021, final version

Table of Contents

Chapter 1: Introduction

Remote sensing encompasses a very wide range of techniques that employ non-destructive methods to observe, explore, and acquire information about the earth without making direct contact with it (Lillesand *et al*. 2015, 1). In archaeology, remote sensing techniques have for decades played a crucial role in the exploration, analysis, and monitoring of archaeological sites (Lasaponara and Masini 2011; Sarris *et al.* 2013, 1454-1456). Archaeologists were quick to recognize the value of collecting data on archaeological sites and features from the air (Musson *et al.* 2013, 17-54; Renfrew and Bahn 2016, 81-85; Rączkowski 2014). By taking a birds-eye perspective, patterns and structures become visible that could normally not be seen by an observer on the ground. In addition, the non-destructive aspect of remote sensing techniques is of great benefit to the field of archaeology and heritage management, which strives to preserve archaeological remains in situ. Excavations and surveys can be expensive, time-consuming, and sometimes even impossible due to a wide range of factors. These issues are (partially) circumvented through the means of remote sensing. There is an ever-increasing quantity of remote sensing data generated by many fields, including the environmental sciences and the military sector. These sources, while not directly related to archaeology, can potentially yield valuable information about archaeological contexts (Lambers 2018, 110). Furthermore, this data allows researchers to see, normally imperceptible, expressions of features in the landscape, such as subtle changes in electromagnetic radiation and magnetism (Hadjmitsis *et al.* 2013, 57-58; Lasaponara and Masini 2011, 1995).

A wide range of remote sensing techniques are employed in archaeology: aerial and satellite imagery, LiDAR, multispectral and hyperspectral imaging, ground-based geophysical methods such as ground-penetrating radar and magnetometry to name but a few (Hadjmitsis *et al*. 56-57; Lasaponara and Masini 2011, 1995; Sarris 2015). In remote sensing, it is important to make the distinction between sensor and platform (Toth and Józków 2016, 23-33). The sensor is the apparatus recording specific wavelengths of energy. The platform is the vehicle or structure carrying and transporting the remote sensor or sensors. I will explain the characteristics, costs and benefits, and applications of different kinds of sensors and platforms in the following chapter.

Since the 1970's, there has been an increasing interest in aerial thermography as a remote sensing method for archaeological prospection (Scollar *et al.* 1990). Aerial thermography is a passive method of remote sensing that records thermal infrared radiation across a landscape from an aerial platform. Due to the differences in composition, density, and moisture content, objects on and beneath the surface can absorb and reradiate long-range thermal infrared radiation at different rates (Casana *et al.* 2017, 311-313; Cool 2018, 1-3). In archaeological contexts, this means anthropogenic features can be perceived if their thermal characteristics are sufficiently distinct from their surrounding soil matrix.

The increased interest in this method is due to the proliferation of consumer-grade Unmanned Aerial Vehicles (UAVs) and low-cost, high-quality thermal sensors (Campana 2017, 277-281). Until recently, thermal remote sensing was an expensive and labour-intensive method, which required an airplane-mounted scanning radiometer (Périsset and Tabbagh 1981, 170; Scollar *et al.* 1990, 611-618). Technological improvements in regards to battery technology, electro-motors, and lightweight cameras have circumvented these issues. Drone thermography builds on an already pre-existing field of airborne and spaceborne thermography. However, it is the higher resolution, lower cost, and ease of use of drones that make the application of thermography so much easier.

In archaeology, more and more case studies are being conducted that apply drone thermography as a prospection and survey method (Casana *et al*. 2014, 207; Casana *et al*. 2017, 314-324; Hill *et al*. 2020; McLeester *et al*. 2018; Salgado Carmona *et al*. 2020; Thomas, 2017). As it stands, more research is needed to refine key factors, such as the timing of thermal surveys, which can greatly influence the quality of the thermal signals of archaeological features. Furthermore, the techniques that can be employed to visualize archaeological features in thermal remote sensing data are understudied.

With this thesis, I will answer the question: *how can drone-based thermography data capture and visualization techniques best be employed to identify archaeological features at the Early Iron Age funerary landscape of Halos?* To structure the process of answering this research question, I have formulated several sub-questions:

1. *What is the current state of knowledge on the archaeological site of Halos?*
2. *What is the current state of drone-based thermography and its application within archaeology?*
3. *What factors influence drone-based thermography data quality?*
4. *What thermal signals can be expected based on the pedology and archaeology at the site?*
5. *How can raster visualizations techniques can be used to analyse drone-based thermography data?*
6. *How can the thermographic signals of the Iron Age funerary landscape of Halos be interpreted, and how do the results compare to the hypothesised thermal signals?*

In this thesis, the site of Halos is used as a case study. Halos is a large, multi-period site located in Thessaly, Greece, which has been the subject of many archaeological investigations (fig. 1.1). In July of 2019, the 4D Research Lab of the University of Amsterdam performed an aerial thermography survey using a drone to investigate the Early Iron Age funerary landscape on the Voulokaliva plain. The data collected during this survey forms the basis for my analysis.

Based on the geology, landscape, and archaeology at the site, and previous archaeological research applying aerial thermography, I will formulate the expected thermal signal of possible archaeological traces. Then, in a qualitative visual assessment of the Halos data, I will apply, compare, and review the effectiveness of different visualization techniques that aid in the identification and visualization of thermal

anomalies. After this, I will compare how the expected signals weigh up against the thermal anomalies identified in the survey, and discuss how conditions during data capture affect the recorded signal.

In chapter two, I build on academic literature to provide the context for my research. In the first part, I will introduce the site of Halos by giving a summary of the geology and landscape in the area. I will provide an overview of previous research and detail the archaeological background of the site. In the second part, I will introduce aerial thermography in detail. I will first introduce the theory behind thermography. Then I will introduce the background of Unmanned Aerial Vehicles (UAVs), discuss the different sensors and platforms that can be utilized in aerial thermography, and highlight relevant case studies applying the technique within archaeology.

In chapter three, I introduce the data and methods that I make use of. First, I go into detail about the particularities of the surveys, specify the sensor and platform used during data capture, and go over the pre-processing steps taken. Secondly, I outline my methodology. I formulate the expected thermal signals of possible archaeological features in the area, and I shortly describe the different visualization techniques I will apply and evaluate.

In chapter four, I present the results of my analysis. First, the general findings will be discussed. After this, the detected anomalies will be interpreted and compared to the formulated expected thermal signals. Lastly, the effectiveness of the visualization techniques is evaluated.

In chapter five, I discuss how my results relate to both the broader archaeological context of Halos and the current state of research into applying aerial thermography in archaeology. Additionally, the data, methods, and results of this thesis are critically examined to discuss their limitations.

In chapter six, I conclude my research by revisiting and answering the research questions posed in this introduction. Furthermore, I summarize the key findings and lessons to take away from this case study, and discuss several recommendations for future research.

Chapter 2: Background

2.1 Case study: Voulokaliva, Greece

In this chapter, I will first examine the geological and landscape context of this region. Secondly, I will detail the excavation history of the site. The results of these archaeological investigations in the area will be summarized according to various key sites. Furthermore, I will examine the Early Iron Age at Halos and the related funerary landscape of the Voulokaliva in detail. For my analysis, it is important to know the geology, land use, and archaeology in the area as these can indicate the possible range of archaeological traces that could be expected. Something to note, Halos often refers to the short-lived Hellenistic polis, which is also known as 'New Halos'. An older site, Magoúla Plataniótiki, has been interpreted as the precursor to the Hellenistic Polis, and is therefore referred to as 'Old' or 'Classical' Halos, or simply also as Halos (Agnousiotis *et al.* 2020, 301; Reinders *et al.* 1991, 88-90). In this thesis, I will use Halos as a proxy for the wider region of these sites. This area encompasses the *chora*, or hinterland, of the ancient polis and stretches out over parts of the Almirós, Soúrpi, and Voulokaliva plains.
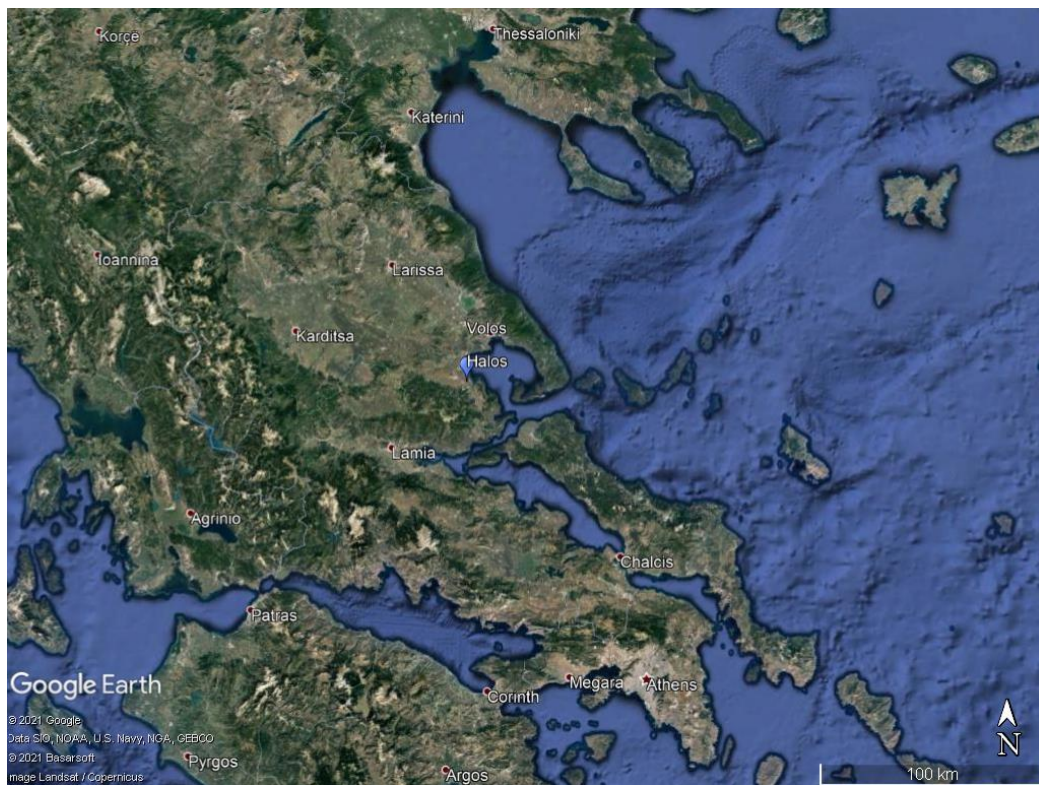
2.1.1 Geology

Figure 2.1: A detail of the map of Greece showing the location of the site in relation to modern Greek cities (Google Earth).

The site of Halos is located in the Magnesia region of Thessaly, Central Greece (fig. 2.1). While the exact genesis of this area has yet to be examined further, it has been concluded that the region was formed during the cyclic growth and decay of the great Quaternary ice sheets (Floras and Sgouras 2004, 6). Their waxing and waning caused isostatic readjustments, changing the relative levels of land and sea. Corings done around the region have shown that the modern waterbody, the Pagasitikós gulf, was a plain containing a large lake until about 13,500 BCE (Reinders 2004, 20). After the end of the Last Glacial Maximum, rapid melting of ice caps caused the sea level in the area to rise to modern-day levels, leading to the creation of the modern-day landscape (Stissi *et al.* 2015a, 91-92; Floras and Sgouras 2004, 6). Two active fault lines can be found along the northern and southern margins of the region. Earthquakes have plagued this region in recent years and it can be assumed that these have also caused damage to earlier settlements.

2.1.2 Landscape

With the Almirós plain to the north and the Soúrpi plain to the south, the Voulokaliva plain slopes gently down to the Pagasitikós gulf (fig. 2.2, below). Several modern towns, notably Neos Platanos and the larger Almiros, are located nearby. To the west of this area lay the foothills of the Othrys mountains, rising gradually over these plains. Nearby to the southeast, a backswamp is located behind a small beach ridge on the gulf. The Voulokaliva plain is flanked by the riverbeds of the Platanórema and Amphrysos, which only carry water in wintertime and after flash floods and transport the sediments from the Othrys mountains. The entire area is in a sense an extensive alluvial slope.
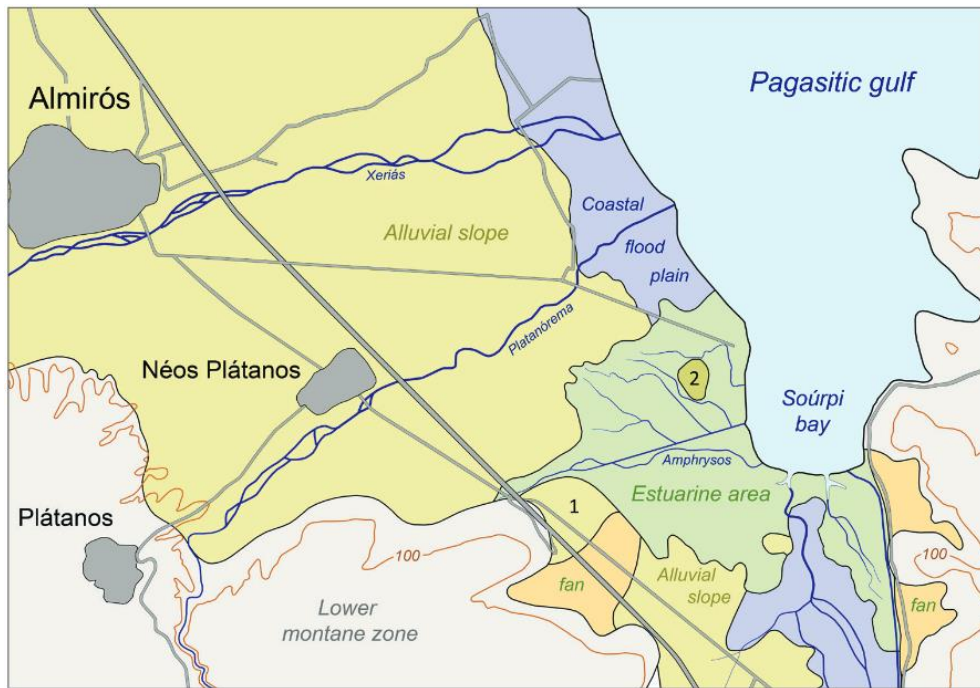
Figure 2.2: The landscape zones and physical surroundings of the region, including modern towns and infrastructure in grey (Reinders 2014, 26). Areas 1 and 2 on the map denote New Halos and Classical Halos respectively.

From the banks of these intermittent rivers, we can gain an insight into the stratigraphy of the area (Reinders *et al*. 1991, 32). The topsoil, a red sandy clay, is made up of a mixed layer of weathered Plio-Pleistocene and fluvio-lacustrine deposits. This layer is intermixed with rounded cobbles and pebbles (Floras and Sgouras 2004, 7; Reinders 2014, 29). Below are alternating layers of red clayey soil, sand, rounded cobbles, and small pebbles. In many parts of this area, these layers show thick, extended development. Due to the high permeability of these soils, underground aquifers have formed in the other plains. Soil samples, collected in augering campaigns between 1996 and 2000, have given us more insights (Floras and Sgouras 2004, 12-18). The samples show that the soil is relatively alkaline and contains very little organic matter. Furthermore, it contains high amounts of phosphorus and calcium carbonate. These soils are fertile and are under heavy cultivation today, with olive groves, vineyards, and fields of cotton and cereals dotting the landscape.

2.1.3 History of Research

Since the early 20th century, this region of Halos has been subject to various archaeological investigations. The region is referenced in several historical and literary sources, including Homer's *Iliad* and Strabo's *Geographies*, which attracted the attention of archaeologists and philologists (Haagsma 2010, 20). One such archaeologist, the Dutchman Carl Wilhelm Vollgraff, conducted fieldwork in the Almirós area to locate the sanctuary of Athena Itonia (Stissi *et al*. 2015a, 87). He excavated various *magoúles*, dwelling mounds, but did not find what he was looking for. He did, however, uncover some settlement remains of Magoúla Plataniótiki, which would later be interpreted as the site of Old Halos (Agnousiotis *et al.* 2020, 301; Stissi *et al*. 2015a, 87; Reinders *et al.* 1991, 36). In 1912, Wace and Thompson from the British School at Athens investigated the Voulokaliva and documented only ten of the tumuli present in the landscape. They created a map and a summary account of the excavation of one of these burial mounds (Wace and Thompson 1912).

The landscape remained relatively undisturbed in terms of archaeological preservation until the late 1960s (Reinders *et al*. 1991, 31). The parcelling of the landscape, coupled with the introduction of heavy agricultural machinery, transformed the region into an agricultural landscape. Deep-ploughing, looting, and the creation of new national roads and industrial areas have threatened the survival of archaeology in the region. Many of the tumuli have been destroyed by mechanical tillage, leaving only scatters of cobbles and sherds (Reinders 2004, 98). These activities prompted new investigations. Starting in 1976, the University of Groningen has been periodically investigating this area in partnership with the Netherlands Institute in Athens and the Ephorate of Antiquities of Magnesia. Their campaign, led by Reinder Reinders, initially focused on mapping and excavating the Hellenistic town and its gate (Reinders 2014). In 1990 they expanded their efforts by initiating the Halos Archaeological Survey Project (HASP). Periodical survey campaigns were conducted in the wider Halos area. These surveys led to the discovery of many new features and finds, including 27 new tumuli in Voulokaliva (Reinders 2004, 94). During the same time, various rescue excavations took place along the Voulokaliva on account of the planned national Highway between Thessaloniki and Athens (Stissi 2011, 151). As of 2011, the University of Amsterdam has joined this partnership and re-surveyed many of the areas previously covered by the surveys in the 1990s (Stissi *et al.* 2015b). During a survey in July of 2019, aerial thermal imaging and

aerial photography were performed with a quadcopter drone. The data generated during this survey forms the basis for my analysis and will be explored in a later chapter.

From these archaeological investigations, a picture of the occupational history of the Almirós, Soúrpi, and Voulokaliva plains can be sketched based on several key sites.
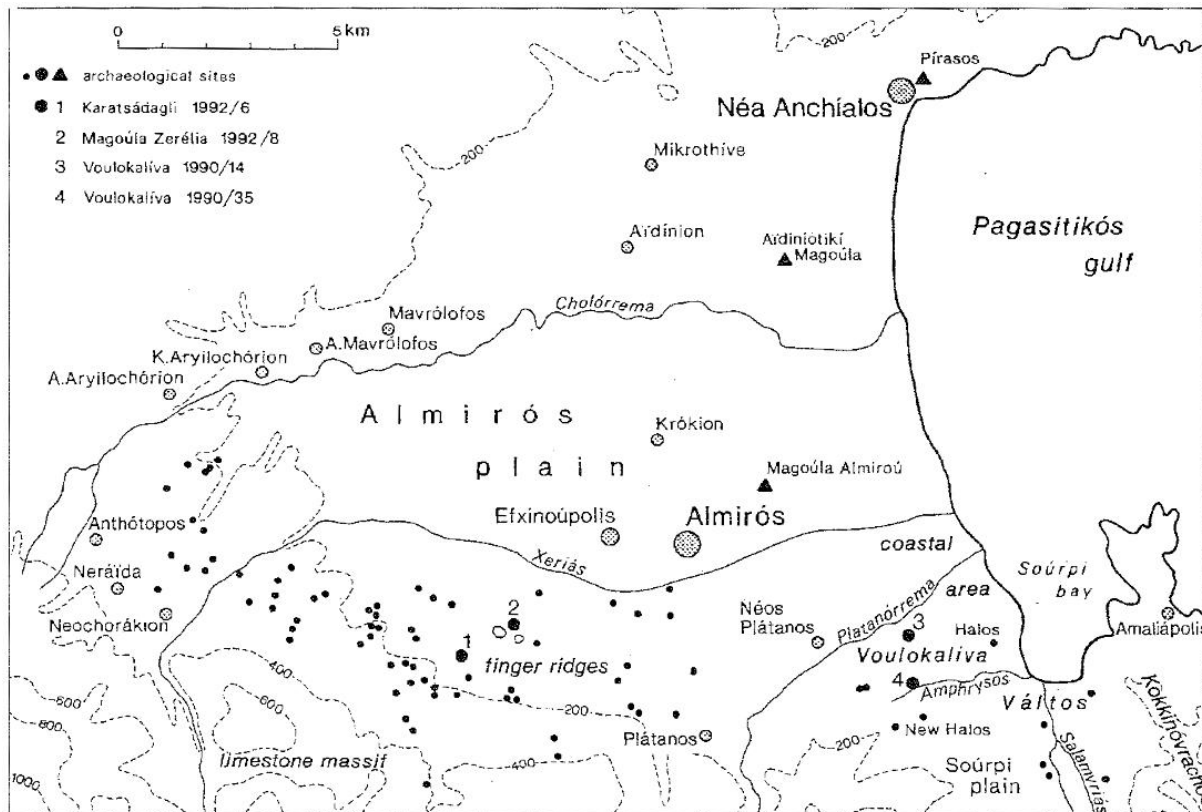
2.1.4 Archaeological context

Figure 2.3: The archaeological sites of the Almirós, Soúrpi and Voulokaliva plains (Reinders 2004, 4). N.B.The church of Ayios Nikolaos is located next to Karatsádagli. Halos, on the map, refers to the site of Magoúla Plataniotiki.

The area (fig. 2.3) has a long cultural history, tracing its occupation back to the early Neolithic (see appendix 1 for a chronology of the sites mentioned in the text). As of yet, no sites belonging to the Palaeolithic and Mesolithic have been discovered. The most probable location for these sites would have been in caves along the southwestern shore of the Pagasitikós gulf, which now lie submerged after the sea levels rose to modern levels (Reinders 2004, 20).

Several well-preserved Early and Middle Neolithic sites have been researched (Reinders 2004, 20-38). While none of these sites have been extensively excavated, surveys have resulted in the collection of surface remains. Karatsádagli is dated to the second half of

the 7th millennium BCE and is the earliest known site in the area (Reinders *et al*. 1997, 104-105). Many artifact types were uncovered in surveys, including pottery, ground and chipped stone tools, and animal remains. Archaeozoological analysis shows that animal husbandry was already in an advanced stage of development (Reinders *et al*. 1997, 129). The Early and Middle Neolithic site of Pirasos, located at the northern periphery of the Almirós and Soúrpi plains, yielded similar pottery finds as Karatsádagli (Wijnen and Rondiri 2004, 37). The settlement mound of Magoúla Zerelia shows a longer occupational history. Based on the pottery that was found, the settlement originated in the Middle Neolithic possibly continuing into the Late Bronze Age (Wijnen and Rondiri 2004, 22-24).

Just above the Amphrysos river, a slightly raised tell named Voulokaliva 1990/35 represents a multitude of periods. Sherds of cookware and storage vessels have been identified as belonging to the Late Neolithic Rachmáni Culture (Christmann and Karimali 2004, 41). This site is one of the few documented sites which shows evidence of the Late Neolithic-Early Bronze age transitions. Pottery, 81 obsidian and flint tools, and 23 ground and polished tools from this period have been examined thoroughly (Christmann and Karimali 2004, 41-74). A relatively small amount of Late Bronze Age material was also discovered at Voulokaliva 1990/35, suggesting a preference for higher-lying areas (Stissi 2004, 91-93). Furthermore, Early Iron Age traces indicate the possibility of renewed habitation (Stissi 2011, 152).

The Magoúla Plataniótiki was a Middle Bronze Age site located on an ancient sand spit in the backswamp on the coast of the Pagasitikós gulf. This site has been presumed to be Classical Halos due to its large size and location near the coast, which is corroborated by literary sources (Agnousiotis *et al.* 2020, 301). Trial trenches in 2013 and 2014 show a continuous habitation sequence, with at the top a stratum belonging to the mid-3rd Century BCE. This stratum suggests a densely populated, well-organized town that could be partially contemporary with New Halos. Various destruction layers underneath the Hellenic stratum, suggest that the town underwent regular earthquake events, but was continually inhabited. It is not yet known whether one of these layers corresponds to the historically documented destruction of this town by the Macedonian General Parmenion in 346 BCE (Dem. Or. 19.163; Agnousiotis *et al*. 2020, 302-303; Reinders 2015, 15; Stissi *et al.* 2015a, 112). There is very sparse evidence of Early Iron Age and

Archaic habitation here, though this has not yet been extensively investigated (Stissi 2011, 152). The sites that have been dated to the Early Iron Age, including the Voulokaliva Funerary Landscape and the possible settlement traces of Voulokaliva 1990/35 and Magoúla Plataniótiki will be described in further detail at the end of this chapter.

The Archaic period, which follows the Early Iron Age, is mostly represented by the site of Voulokaliva 1990/14. The site produced pottery fragments dating to the 6th Century BCE. Also, some of the tumuli yielded pottery remains dating to this period. This suggests they were in use for a longer period than initially expected (Stissi 2004, 116-117). Why Archaic finds seem to be largely absent from the archaeological record of the area has as of now not been determined.

The Hellenistic period is best represented by the polis of New Halos. Modern interpretations of historical sources put the foundation of this Hellenistic city around the end of the 4th century BCE or the beginning of the 3rd century BCE (Haagsma 2010, 22-24). This heavily fortified town consisted of a rectangular lower town, with a built-up area of roughly 40 hectares, and an upper town, surrounded by a triangular enceinte that ended in an acropolis. One hundred and eight towers protected the city, together with two large gate structures. The polis was short-lived, however, as an earthquake caused extensive damage to the city around 265 BCE, which led to the abandonment of the city. The area of one of the gates showed evidence of continued occupation after the city was abandoned.

The wider Halos region did not contain any large Roman towns or ports, as the region was overshadowed by the nearby towns of Phtiotic Thebai, Demetrias, and Pharsalos (Reinders and Prummel 2003, 19-20). This is mirrored in the small amount of finds dating to this period, which suggest New Halos was marginally reinhabited during the Roman period (Reinders 2014, 25). Around the 12th and 13th centuries, the port city of Almiros (or Armiro) was said to be one of the principal harbours of the Byzantine Empire (Reinders and Prummel 2003, 20-22). This city was located on the coastal part of the Almirós plain, east of where the modern town of Almirós is located, and is supposed to have housed communities of Venetians, Genoans, Pisans, and Jews. In addition, a Byzantine stronghold was built on top of the remains of the acropolis of New Halos.

The small church of Ayios Nikolaos currently stands ruined atop a hill overlooking Karatsádagli. It was built in 1818 when the region of Thessaly belonged to the Ottoman Empire (Reinders *et al.* 2008, 85-89). Many of the building materials show reuse from Hellenic, Roman, and Byzantine times.

Due to the time-depth of some sites in Halos, with areas like Magoúla Zerelia showing continuous occupation throughout various periods, it can be concluded that the habitation patterns and settlement preferences on the Almirós, Soúrpi, and Voulokaliva plains were remarkably stable. This seems rather unusual for Greece, where many sites do not show similar levels in the long-term continuation of settlement patterns as can be found here (Stissi *et al.* 2015a, 74-75).

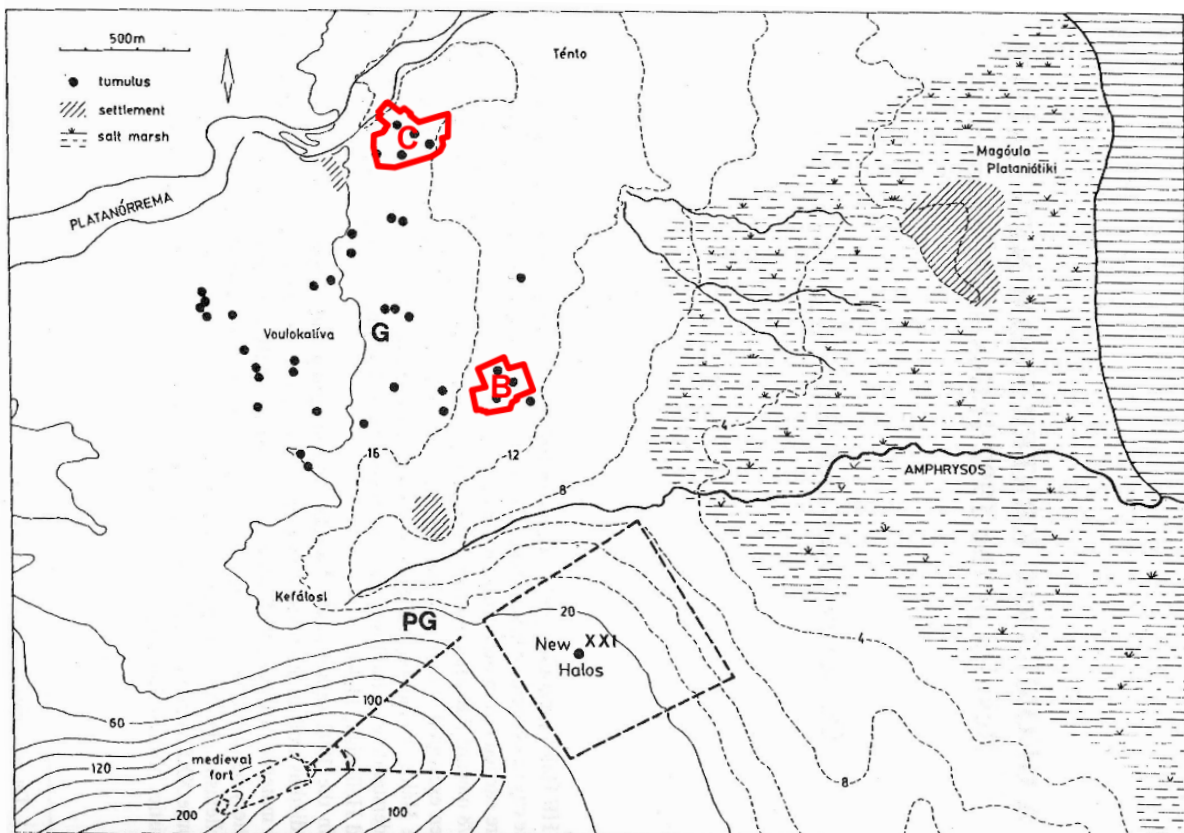### 2.1.5 The Early Iron Age sites on the Voulokaliva

Figure 2.4: The Voulokaliva plain, with the city of New Halos and Magoúla Plataniótiki (after Reinders 2004, 95). Overlaid are sites B and C which were covered in the survey during July of 2019.

The Early Iron Age in Halos is most notably exemplified by the necropolis on the Voulokaliva plain (fig. 2.4). The funerary landscape encompasses 2.5 km^2 and contains no less than 37 burial mounds. The inhabitants of Halos started cremating their dead

around the end of the Protogeometric period (c. 900 BCE), covering the cremation pyres with cairns of stones and then erecting a tumulus over them (Georganas 2002, 289). The study of the artefacts discovered around these mounds indicated that the tumuli in the Voulokaliva area were used for a long time, at least until the Archaic period (c. 500 BCE).

Figure 2.5: The interior of the excavated Mound 36 on the Voulokaliva plain (Lagia et al. 2013, 203).

Several of these tumuli have been excavated, and from these, we can glean insights into how these structures were designed. Wace and Thompson excavated 'Tumulus A' in 1912. They discovered the remains of 19 cremation pyres and an additional eleven cist graves that were added later (Wace and Thompson 1912). This structure inside the tumulus was built from rounded cobbles and irregularly shaped limestone slabs. In turn, these slabs were covered with the red Pleistocene sandy clay. Cobbles, boulders, and other stones capped the mound. In 1999, Mound 36 was extensively excavated (fig. 2.5) (Lagia *et al.* 2013, 203-208). This tumulus is one of the more elaborate in this area. The nearly circular mound measured 30.6 by 30.2 meters and was 1 meter high at its peak. The entire pile was covered by large capping stones. Inside, a large beehive-like structure comprised of concentric 'precincts' that stored cremated and inhumated remains. The core of this structure is dated to the Sub-Protogeometric. Stone-lined pits were added at later dates throughout the Geometric and Archaic periods. Rich grave goods, such as pottery, iron weapons, iron and bronze jewellery, and bronze bowls, were present in many of the precincts, as well as offering tables and grave markers (*semata*) (Rehren *et al.* 2006, 207). In total 98 precincts, 4 (possible) domed tholoi-like structures, 3 urns, 16 infant and 4 adult inhumations were discovered. Both Tumulus A

and Mound 36 are relatively large tumuli and present a relatively rich view of these features. In general, most tumuli will have a layer of cobbles covering their insides but might vary in the density of graves included within them.
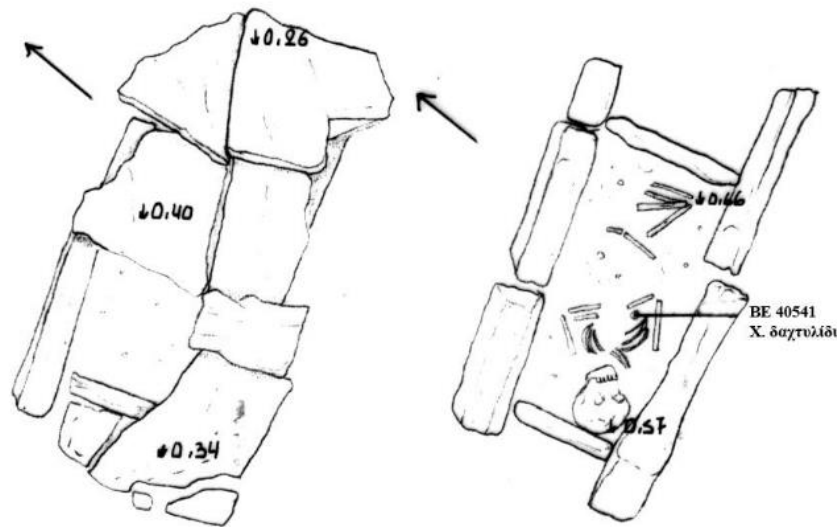

Figure 2.6: An example of a single grave found in the excavation along the national highway in the area (grave 17, Tsiouka 2008, 226). Shown on the left is the slab covering. On the right is the interior of the grave.

While the mounds may be the most obvious of the Early Iron Age features in the Halos area, they are not the only funerary practice in the area. The funerary landscape seems to have extended further south (Stissi 2004, 102). Rescue excavations along the narrow stretch of the planned national highway revealed the presence of 141 single graves (fig. 2.6). These did not have an explicit expression in the relief of the landscape and were never spotted in previous surveys (Stissi 2011, 152). The majority of them date to the Protogeometric and Geometric periods of the Early Iron Age. These graves were lined and covered with limestone slabs to form cists, and appear both isolated and in clusters. However, they do not seem to be ordered along a common axis (Tsiouka 2008, 87). There is quite some variability to these single graves. For example, the depths at which these features were discovered range from less than 35 centimetres beneath the topsoil to depths up to 171 centimetres (Tsiouka 2008, 221-249). Several burials contained the remains of not one, but multiple people. Grave goods like ornaments, pottery, and weapons were also present in many of the burials (Tsiouka 2008, 6-7, 25-79). In the same excavation, three additional tumuli were discovered too.

Because of the impressive remains of this funerary landscape in the Voulokaliva area, it raises the question of whether there was also a related settlement. This brings us to two other non-funerary sites. Both Voulokaliva 1990/35 and Magoúla Plataniótiki yielded Early Iron Age remains. Voulokaliva 1990/35 shows a much larger concentration of finds than any of the funerary concentrations. The Early Iron Age finds from Voulokaliva 1990/35 show no traces of burning (in cremation pyres). While it has not been excavated, the area has been interpreted as either a possible settlement site or as playing a role in the funerary practices in the area. It should be noted that the size of the area is quite small, especially if it would have been used as a settlement (Stissi 2011, 152). Magoúla Plataniótiki shows a minor concentration of sherds from this period. However, the distance to the funerary field makes it an unlikely contender for an Early Iron Age settlement site. The question of an Early Iron Age settlement remains unanswered.

All in all, outside of the necropolis there seems to be a relative absence of Early Iron Age sites and find material. In his analysis of the Early Iron Age traces from both Halos and Tanagra, a Boiotian settlement, Stissi (2011, 149-150) brings up various possible explanations for this absence. There is a possibility that the surveys in the 1990s did not examine the correct areas to find remains from this period. The surveys in Halos focused mostly on the most accessible areas (Reinders 2004, 3-6). This left out much of the foothills, backswamp, and other remote areas. Furthermore, an entire category of features, the single graves, did not produce any noticeable expression in the landscape. This made them easy to miss during surveys. Another possibility is that most of the Early Iron Age traces have been destroyed. The brittle nature of sherds from this period, combined with bad preservation due to continued habitation of the same areas and mechanical tillage of the landscape, has led to much of the archaeology being destroyed.

Now that the background of the site has been discussed in-depth, it is time to focus on the science behind thermography, its archaeological relevance and its application as a remote sensing method.

2.2 Thermography

Thermography, also known as thermal imaging or thermal prospection, is a remote sensing technique that relies on the sensing of thermal infrared radiation (TIR) – or more generally, heat - across a landscape.

TIR is part of the infrared range of the electromagnetic spectrum and is emitted as an electromagnetic wave (fig. 2.7, below). The wavelengths of the infrared range (0.76-1000 µm) are longer than those of visible light (0.4-0.76 µm), and therefore invisible to the human eye (Dumoulin 2017, 234). Thermal infrared radiation commonly occupies a range of 8-15 µm wavelengths, but atmospheric windows also allow TIR to be sensed in the 3-5 µm range. It should be noted that the 8-15 µm range is preferred for thermal imaging as this range allows the ground temperature to be measured without interference from the ambient air temperature (Cool 2015, 5; Kuenzer and Dech 2013, 5).
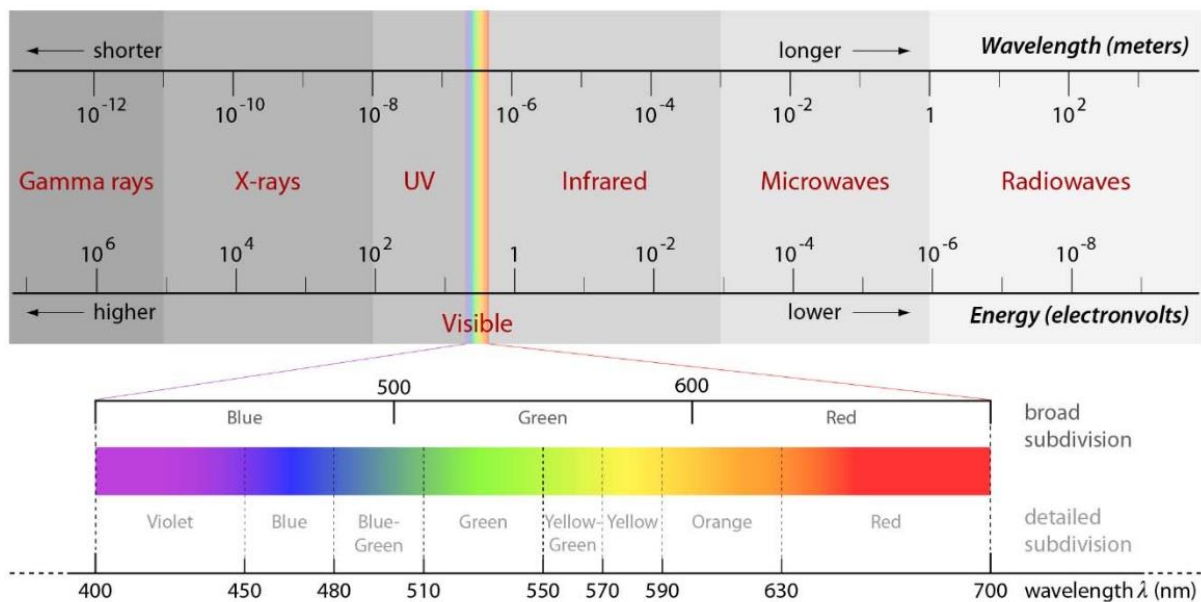

Figure 2.7: The complete electromagnetic spectrum (Verhoeven 2017, 15).

All objects with a temperature above absolute zero (0 K, which equals -273 °C) emit TIR (Kuenzer and Dech 2013, 1). The source of this type of radiation is the sun. Much of the sun's energy is reflected back into space by the earth's atmospheric gasses. The TIR that does pass through the atmosphere is absorbed and reflected by objects on and near the surface of the earth at different rates (Abrams and Comer 2013, 60-63). Due to the differences in composition, density, and moisture content, these objects and materials have distinct thermal behaviours over a 24-hour cycle (fig. 2.8, below) (Casana *et al.* 2017, 311-313; Cool 2018, 1-3; Dumoulin 2017, 237-241).
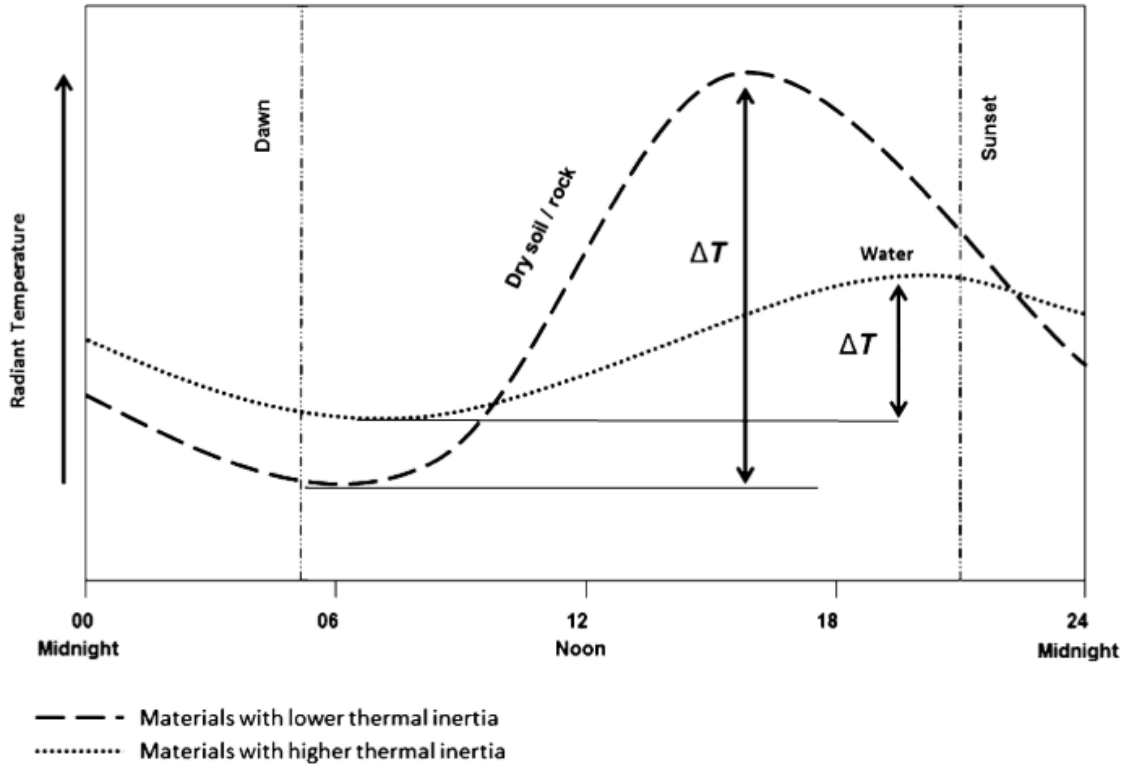
Figure 2.8: Hypothetical illustration of the relative thermal radiance of dry soil versus water (or saturated soil) over the diurnal cycle (Kuenzer and Dech 2013, 18).

2.2.1 Thermal behaviour

Four thermodynamic properties affect these thermal behaviours: thermal conductivity, diffusivity, volumetric heat capacity, and thermal inertia (Cool 2015, 7-16; Cool 2018, 1-3; Casana *et al.* 2017, 311-313). Thermal conductivity describes the quantity of heat that can be transported through an object or material. To detect subterranean archaeology, the superficial ground layer has to be sufficiently conductive, as enough heat needs to be able to penetrate to the depth of the feature (Périsset and Tabbagh 1981, 170-171). Between particles of dry soils, spaces of low-conducting air are present. This restricts the transfer of heat. If the amount of water in the soil increases, this air is replaced by water. This increases the points of contact between soil particles, in turn improving the conductivity of the soil. It should be noted that the amount of conductivity in soil decreases as the organic content increases and as the size of the soil particles decreases (Cool 2018, 1; Stanjek and Faßbinder 1995, 97).

Diffusivity describes the effectiveness with which an object or material conducts thermal radiation. While it may seem similar, the difference between thermal conductivity and diffusivity is that thermal conductivity describes the *quantity* of heat that can be

20

transported through an object, whereas diffusivity describes the *rate* with which heat is transported through an object (Cool 2018, 2).

Volumetric heat capacity describes the amount of thermal energy that a given volume of an object must absorb to change the temperature of that object by 1 °C. This property accounts for the density and natural heterogeneity of soils (Casana *et al.* 2017, 311). As density increases, so does heat capacity (Cool 2015,16). This is why dense materials, like rocks, will be warmer than loose materials, like soil, when exposed to the same heating conditions.

Thermal inertia is the ability of an object to resist changes in temperature. It is a useful value for estimating the potential strength of anomalies in different contexts (Cool 2015, 9). This behaviour is most visible after a change in the direction of heat flux (fig. 2.8, above). In essence, heat flux is a variation in temperature. There is positive heat flux when the soil is warming, and negative when it is cooling. The primary type of heat flux comes from the diurnal cycle. After direct heating during the day, cooling starts at sunset and differences in thermal inertia become apparent. There are also periods of transient heat flux, which are sudden reversals in the direction of heat flux (Casana *et al.* 2017, 314, 316; Hill *et al.* 2020, 17). It has been speculated that these periods can provide some of the starkest contrasts in thermal inertia (Cool 2015, 15; Cool 2018, 4). The moment of capture in thermography is therefore of great importance.

2.2.2 Archaeological relevance

Archaeological sites and features can consist of a mixture of different types of materials. Examples of these include stone walls, infilled ditches, ancient field boundaries, scatters of ceramics or flint, and earthworks. If thermal imaging is performed at a moment when the thermal signatures of archaeological features are sufficiently distinct from the soil matrix in which they are embedded, it is possible to locate these archaeological features. The resulting image of such a thermal survey is called a 'thermogram'. By analysing these thermograms for anomalous patterns of warm and cool areas, various types of archaeological features can be distinguished (fig. 2.9, below) (Cool 2015, 6; Casana *et al.* 2017, 311).
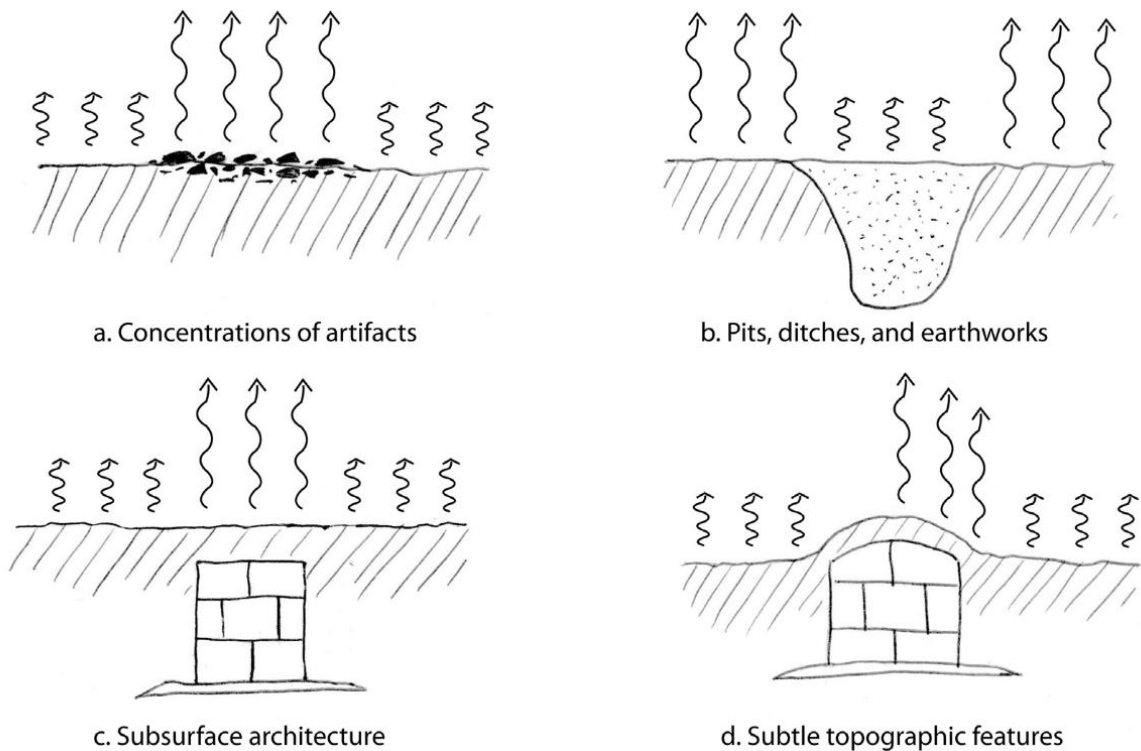
*Figure 2.9: An illustration of possible thermal expressions of various archaeological features. The longer the arrow, the hotter their expected signal is (*Casana *et al. 2012, 312).*

Artefact scatters on the surface can be detected if their thermal signature is sufficiently distinct from the ground cover (fig. 2.9, A) (Casana *et al.* 2017, 311).

Features that have been filled in, such as pits and ditches, which produce no topographic expression can also be detected due to their differing soil composition and moisture-retaining properties from the surrounding soil (fig. 2.9, B). As these features tend to retain water better, the temperature of these wet soils will remain more constant compared to dry soils. This is due to the high thermal inertia of water (Cool 2015, 16; Casana *et al.* 2017, 311).

It is possible to sense subterranean archaeological features using thermal imaging, but this requires various environmental conditions (fig. 2.9, C). Firstly, a conductive superficial ground cover is required, as enough heat needs to reach the level of the feature. Secondly, if the superficial layer is highly diffusive, subterranean features will be affected by heat flux more quickly. However, as the thickness of the superficial layer increases, the strength of anomalies will weaken (Périsset and Tabbagh 1981, 171). In addition, the potential strength of a subterranean thermal anomaly depends on the

relative thermal inertias of the feature and its surrounding soil matrix. Subterranean features are best distinguished when the relative temperature difference between features and the surrounding soil matrix is at its greatest. This is the case after a reversal of the direction of heat flux (Périsset and Tabbagh 1981, 172-175; Cool 2018, 2-3). For example, after a period of stable warm temperatures, all materials will reach their thermal equilibrium. If this is followed by a rapid drop in temperatures (i.e. in a period of transient heat flux), buried features, even at depths of up to a meter below the soil, will be at their most visible (Scollar *et al.* 1990, 597-598; Casana *et al.* 2017, 312-313).

If the surface topography reflects subsurface features - a slight ridge over a buried wall or a slight depression relating to a ditch - these can show up in thermographic surveys. Topographic features have different thermal properties than surrounding flat ground and will therefore heat and cool faster (fig. 2.9, D). Solar radiation will strike these features obliquely at sunrise and sunset, and due to this exposure, they are very discernible in thermal imagery (Cool 2015, 13; Casana *et al.* 2017, 311). In the same way, topography on the surface can add noise to the image if it is unrelated subterranean features (Scollar *et al*. 1990, 601).

2.2.3 Sensors and platforms

To perform any type of remote sensing, a sensor and a platform are required. In thermography, a thermal camera acts as the sensor. Thermal cameras can be either active or passive. The difference here is that active thermal cameras illuminate an area of interest using short-wavelength infrared, and then record the reflected energy. Passive thermal cameras only record emitted thermal infrared from the area of interest (Toth and Józków 2016, 30-33). For the purposes of aerial thermography surveys, passive thermal cameras are more common (Adamopoulos and Rinaudo 2020, 17; Dumoulin 2017, 238-241).

Thermal cameras have come a long way since their inception. Thermal infrared imagers were originally created for military purposes (Adamopoulos and Rinaudo 2020, 17). In archaeology, the first applications of thermography in the 1970s and 1980s saw the use of large, low-resolution, and expensive scanning radiometers on planes to conduct aerial surveys (Périsset and Tabbagh 1981, 169-170). These sensors required constant cooling with liquid nitrogen and recorded the data on long rolls of film. Nowadays, many modern thermal cameras utilize uncooled microbolometers to sense TIR. This has made

these sensors much more lightweight and affordable, which has led to them becoming widely accessible for commercial use (Adamopoulos and Rinaudo 2020, 1).

The quality of thermal cameras, and the thermograms they produce, is best indicated by various types of resolution. The temperature resolution refers to what temperature increments the camera is capable of detecting (Cool 2015, 17). If the temperature resolution is high, it means that a thermal camera can discern and differentiate between very close temperature levels. Spectral resolution describes the range of wavelengths that the thermal camera records (Abrams and Comer 2013, 64). Most thermal cameras record the 8-15 µm range due to the reasons discussed previously in section 2.2. Radiometric resolution relates to the bit-depth of a sensor (Abrams and Comer 2013, 65). This describes the ability of a sensor to record many levels of brightness. Most thermal data is encoded to an 8-bit resolution. This means that the temperatures on a thermogram are assigned to 256 (= 2^8) shades of grey. An important thing to note is that the grey values of a thermogram are assigned on a relative scale based on the range of temperatures within the image (Cool 2018, 3). This means that thermal cameras do not consistently use the same grey value for the same temperature.

In contrast to the sensors used in multispectral remote sensing, thermal cameras can record data independently of the time of day. This is because multispectral remote sensors only record *reflected* radiation (Kuenzer and Dech 2013, 5, 12-15; Abrams and Comer 2013, 59). A source of illumination (like the sun) is required for radiation to be reflected. As a consequence, multispectral remote sensing is not an option during the night-time, while TIR remote sensing does have this operational flexibility.
The platform carrying a remote sensing instrument should be regarded as of equal importance to the sensing instrument itself (Toth and Józków 2016, 23). For thermography, many different platforms have been used, all with their respective advantages and disadvantages. When a thermal camera is mounted on an aerial platform, the remote sensing technique is often referred to as 'aerial thermography'. As the first thermal imagers were very large, surveys were initially performed using aircraft (Casana *et al.* 2017, 313). The costs of conducting plane surveys were often prohibitive, but did provide coverage of large areas. Satellites carry thermal sensors too but offer lower resolutions and less control over the moment of capture. Satellite imagery does however cover a very large effective area. Studies have been undertaken using handheld

thermal cameras. The resolution provided by this platform is very high, but here the effective area that can be covered in a survey is severely limited (Buck *et al*. 2003, 975-977). Kites have also seen use in remote sensing. These are relatively cheap platforms as they can be independently manufactured and provide simple launching and landing procedures due to their tethered nature. The main drawback is that kites are very much dependent on favourable wind and environmental conditions (Duffy and Anderson 2016, 355; Giardino and Haley 2007, 57). In modern applications of thermography in archaeology, thermal cameras are often mounted on unmanned aerial vehicles (UAVs) to circumvent some of the disadvantages of the aforementioned platforms (Adamopoulos and Rinaudo 2020, 1).

UAVs, or more commonly known as drones, have in recent decades benefitted from technological improvements which have led to their proliferation in commercial use. Their low cost has led to these platforms being picked up in many academic fields, including archaeology. There are two main types of UAVs: fixed-wing and multi-rotor. Both types have their benefits and constraints (Adamopoulos and Rinaudo 2020, 13). Fixed-wing UAVs can perform longer, more stable flights, which is useful in covering extensive archaeological sites or landscapes. They are however less compact and cannot carry the same payload as multi-rotor drones. These systems, while shorter in range, can hover and vertically take off. This increases their ease of use. Furthermore, their larger payloads allow for more flexibility in regards to larger sensor types and gimbals for image stability.

All in all, drones offer great operational flexibility. With their option for autonomous flying along pre-defined paths, drones allow for the systematic collection of aerial data at specific altitudes with precise camera orientation at any time of day and in a range of weather conditions (Casana *et al.* 2014, 208). This is especially valuable for thermal imaging, in which the timing of the flight is of high importance. Using drone platforms for archaeological surveys allows data to be gathered at a lower ground sampling distance (GSD), meaning a high spatial resolution. As with any platform, drones have limitations too. In various parts of the world, there are many restrictions on the use of drones in the airspace (Hill 2013, 29). The battery life of a drone can act as a limiting factor in the amount of ground that can be covered during surveys. Furthermore, the optimal altitude at which a drone operates is still heavily debated. Especially for aerial

thermography, a trade-off must be made between low- and high-altitude flights. Flights at lower altitudes provide a higher resolution, but more images are needed to cover a similar area as a higher altitude flight. The point is, the optimal application of drones as survey platforms depends on the requirements and context of the project. Proper care should therefore be taken in selecting the right tool for the job.

2.2.4 Prior applications in archaeology

In archaeology, multiple case studies have already taken place employing drone-based thermography as a prospection method. I am limiting this discussion to a handful of cases that are relevant to this thesis from recent years. For an overview of the application of this technique in archaeology going back to its advent, it is recommended to read through the thesis by Autumn C. Cool (2015, 19-33).

The paper by Casana *et al*. (2017) summarizes the results of several investigations in North America, the Mediterranean, and the Near East. Especially the investigation at Kalavasos, Cyprus, is of relevance. Here, an aerial thermography survey was conducted on a clay soil, similar to that of Halos, which had received no precipitation since the previous spring. Thermal imaging did not reveal anything of archaeological interest (Casana *et al.* 2017, 316-318). Even while close to the surface, the dry stone architecture had effectively the same thermal properties as the dry soil. This illustrates the importance of soil moisture as a key factor in the visibility of archaeological features in aerial thermography.

McLeester *et al.* (2018) applied drone-based thermal imaging in combination with multispectral, and visible light imagery at Midewin National Tallgrass Prairie, in Illinois, to survey a late prehistoric village. Using these techniques, they were able to discern a range of previously undiscovered settlement traces. It was found that by applying a Principal Component Analysis to a combined dataset of thermal and multispectral images, the archaeological features could be easily discerned (McLeester *et al*. 2018, 454-455). This technique is used in my analysis and explained in the following chapter. Additionally, on the thermal imagery a large hexagonal enclosure could be identified which was not visible on any of the other data (McLeester *et al*. 2018, 457-458). This enclosure is likely to be associated with earthworks which have all been levelled by

intensive ploughing, demonstrating the possible effectiveness of thermography in identifying destroyed archaeological features.

Hill *et al.* (2020) surveyed the Enfield Shaker Village in New Hampshire, USA, using thermal and multispectral imaging, and traditional terrestrial geophysical methods of magnetometry and ground-penetrating radar (GPR). Because the Enfield Shaker Village has significant documentation of potentially visible buried features, this study served as a good test case to compare the techniques. It was found that the visibility of thermal anomalies was highest on images collected after dusk and until several hours after sunset. They attribute this fact to the effects of early-morning dew (Hill *et al.* 2020, 9-11). The surface moisture acts as a 'thermal blanket', quenching the signals with its high thermal inertia. When comparing aerial thermography to the geophysical data, they found that thermal images, under favourable conditions, were able to reveal various features, such as historic pathways, much more distinctly than traditional geophysical techniques (Hill *et al.* 2020, 14). Furthermore, Hill *et al.* provide a technique of removing thermal drift from thermograms which will be discussed in the next section (Chapter 3).

Salgado Carmona *et al*. (2020) performed thermal and multispectral survey at the Iron Age hillfort of Villasviejas, in Cáceres, Spain. In contrast to the previously discussed studies, these researchers employed a quantitative method in their analysis to detect buried structures. To distinguish noise from signal on the thermograms, statistical tests were performed to study the similarity or dissimilarity across various thermal images (Salgado Carmona *et al*. 2020, 4-8). Surprisingly, the thermograms with the highest visibility of archaeological features were captured at noon (Salgado Carmona *et al*. 2020, 9). This contrasts with the results of most other thermal surveys, which recommend avoiding daytime flights due to the possibility of recording reflected thermal infrared radiation. This settles that the optimal timing for thermal data capture has not been answered definitively. After their analysis, archaeological excavations took place to validate their findings. They found a very clear correlation between shallower structures and stronger signals (Salgado Carmona *et al*. 2020, 10).

Now that the theoretical background for both the site and the technique of aerial thermography has been established, I will introduce the data and methods of this research in the next chapter.

Chapter 3: Data and Methods

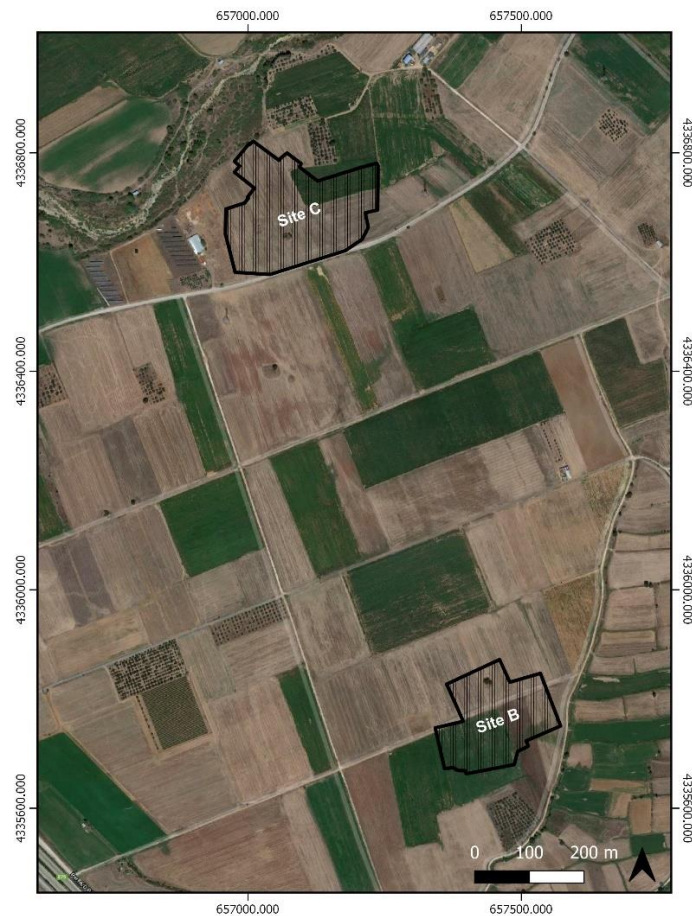## 3.1 Data and Pre-processing

Figure 3.1: Site B and site C on the Voulokaliva plain.

In this thesis, I will be using the data collected in a survey employing aerial thermography during July of 2019 at sites B and C on the Voulokaliva plain in Halos (fig. 3.1). Using a drone, various flights were undertaken across different parts of the day, in various weather conditions, and at different altitudes (table 2, next chapter). Both thermal and optical - visible-light - images were captured. To allow for accurate georeferencing, ground control points (GCPs) in the form of aluminium squares were placed in the field, and their locations were recorded using a DGPS. Aluminium was used as this shows up very distinctly on the thermal images due to its high reflective capability. It should be noted that the area within the sites covered by each flight varied to a certain extent.

Figure 3.2: The UAV system (left) and thermal camera (right) used during the thermographic survey at Halos (DJI 2017; DJI 2018).

The drone that was used during the survey is the DJI Matrice 210 (fig. 3.2, left) (DJI 2017). The flights were planned so the images were captured with 70-80% overlap. Thermal images were captured using the DJI Zenmuse XT2 thermal infrared camera (fig. 3.2, right) (DJI 2018, 15-17). This passive sensor captures uncooled radiometric 14-bit still images at a pixel resolution of 640x512 and a spectral resolution of 8-15 μm. Furthermore, this camera also possesses an integrated optical camera with a 12-megapixel sensor, which captures images at a resolution of 3840x2160 pixels. Both cameras use a global shutter, which, especially in drone data capture, is important in avoiding the 'rolling shutter effect'. Rolling shutters in cameras capture images by scanning across a scene rapidly. Due to the speed at which a drone is moving, a rolling shutter would cause distortions. Global shutters counteract this by capturing the entire frame at the same time. Due to the thermal sensor being uncooled and operating in a hot climate 'thermal drift' occurred on some of the images. As the core temperature of the camera changes, the absolute temperature values change from image to image during the course of the survey. Therefore the thermal images had to be calibrated to get a more accurate result during pre-processing. This was done by correcting the raw data with the atmospheric temperature and moisture data.

The images captured during the flights were pre-processed into several raster products: a Digital Elevation Model (DEM), a thermal orthomosaic, and an optical orthomosaic. The photogrammetry software 'Pix4D Mapper' was used to produce these (www.pix4d.com). By adding sets of overlapping images to this software, common 'tie

points' are identified. This software then triangulates the relative 3D position of these tie points. From all these triangulated points, a 'sparse point cloud' is constructed. By creating stereographic depth maps for every pair, more tie points are added which results in a 'dense point cloud' and a meshed 3D model. The models were georeferenced by tagging the GCPs on the images.

Afterwards, these models were imported to QGIS 3.10.6 as GeoTIFF files. Following the method outlined in Hill *et al.* (2020, 7-8), the thermal drift was largely removed using a simple raster calculation. First, the mean thermal value for a large area around each cell in the thermogram was calculated to produce a raster dataset that shows the major temperature drift trend from one end of the survey to the other. This trend is then subtracted from the original raster to enhance local contrast and remove the thermal drift.

3.2 Methods

In this thesis, I take three steps. Firstly, I formulate the expected thermal signals of archaeological features. Secondly, in a qualitative manual assessment, I apply various visualization techniques to the data to assess their effectiveness in highlighting thermal anomalies. Thirdly, I will compare how these expected signals weigh up against the thermal anomalies of potential archaeological origin discovered on the thermograms and discuss how conditions during data capture affect the recorded signal.

In my qualitative investigation, I use the optical orthomosaic and DEM as visual controls for the area to ensure a thermal irregularity is not caused by unrelated factors or materials. A qualitative approach was decided on due to the relatively small size of the surveyed areas and the scope of this bachelor's thesis. A semi-automated approach has been tried and seen some success in a thermal survey in Villasviejas, Spain (Salgado Carmona *et al.* 2020, 6-7).

3.2.1 Thermal signals of expected archaeological features

The reason for creating a hypothesis on possible thermal signals of archaeology in the area is to aid in the identification and interpretation during the qualitative visual assessment of the data. Furthermore, by doing this I can compare how our current understanding of thermographic signals relates to the actual situation in the field.
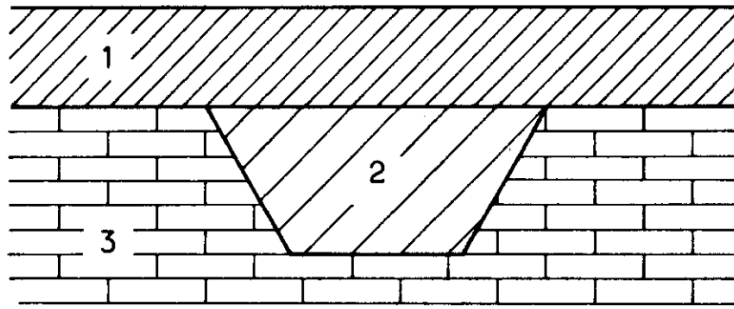
Figure 3.3: A (hypothetical) simplified cross-section of (1) the superficial ground cover, (2) a subsurface archaeological feature, and (3) the surrounding soil matrix (Périsset and Tabbagh 1981, 171).

The thermal characteristics of the landscape should be considered when formulating the expected thermal signals of archaeological features. In the Voulokaliva area, red sandy clay acts as the superficial ground cover (fig. 3.3, 1) (Cool 2015, 48-49). Sand is highly conductive, and when compared to clay it is large-grained and more porous. This provides sand with a low heat capacity, high diffusivity, and very low thermal inertia. Thermal energy can quickly travel through the highly diffusive matrix, which allows subterranean features with high thermal inertias to become visible. Clay has been observed to provide the opposite result (Cool 2015, 50-51). Due to its fine grains, dense structure, and high moisture content, clay has a very high heat capacity, low diffusivity, and very high thermal inertia. This allows the clay to act as a barrier to the thermal signals of subsurface features. The thermal surveys were conducted on agricultural fields that were harvested, leaving inactive vegetative remains on the superficial ground cover. These remains have poor conductivity and can therefore obscure features below them (Cool 2015, 15). All in all, there is quite a possibility the soil at the site will mask thermal signals coming from subsurface features.

The most visible features on the Voulokaliva plain are the tumuli. While most have been damaged by mechanical tillage, some remain as a muted topographic expression in the landscape. If their expression in the relief is distinguishable, the oblique angle of insolation during sunrise and sundown can highlight the tumuli in thermal imagery. Furthermore, the tops of the destroyed tumuli are scattered with pebbles and cobbles presumed to have been used to cover these features in ancient times (Reinders 2004, 98). Inside the tumuli, slabs and cobbles were present, covering the burials. These slabs and cobbles have a high heat capacity, meaning thermal expressions of any possible structures or grave goods below this layer would be more difficult to identify. The

subsoil of the plain, which acts as the surrounding soil matrix (fig. 3.3, 3), similarly contains large amounts of cobbles and pebbles. Because of this, the subsurface remains of the tumuli could get lost masked in natural thermal noise.

The single graves discovered thus far produced no expression in the landscape and were never spotted during field surveys. Hypothetically, it would be possible for these to be visible in thermal imagery. A large number of single graves uncovered at Halos were covered by a relatively thin layer of top soil. At their depth, it is possible that diurnal heat flux can affect these single graves, allowing them to be distinguished on the thermograms. There is a possibility is that the graves are located deeper in the soil. In this case, the thick surface layer can attenuate the signals of features beneath it. The cists within some of the graves were made of several slabs of limestone, which lined the inside and top of the grave. As limestone is a dense material with high heat capacity, it should theoretically be possible for it to be discernible in the sandy clay ground cover. However, the previously mentioned cobbles and pebbles included in the soil could also act as thermal noise for this feature. It should be noted that, as the surveys were conducted over agricultural fields, there exists a great possibility that many of the subsurface features were destroyed by ploughing. The process of ploughing can bring scattered remains (e.g. fragments of limestone slabs or pebbles) to the surface. Surface scatters are therefore an important indicator of the presence of archaeology in the area. Due to their contrasting characteristics with the natural soil, these can most likely be sensed as concentrations of warm signals using thermography.

As a summary, the expected signals have been formatted in a table (table 1, below).

Archaeological feature	Hypothesised thermal signal
Tumuli	• Stone cover is visible as a **large warm thermal signal**, internal structure beneath this cover will be masked. • If the tumulus has a topographic expression, the exposed side will show a **high thermal signal** due to oblique insolation.
Single graves	• If the graves are close enough to the surface and are not damaged: **visible as warm areas**. (These could be masked by subsurface inclusions). • If the graves are located deeper or significantly damaged: **not visible on the thermograms.**
Surface scatters	• Visible as **concentrations of small warm signals.**

Table 1: A summary of expected archaeological features at the site of Halos and their hypothesised signal on the thermal images.

3.2.2 Visualization techniques

Visualization techniques can facilitate the identification of patterns in the data. Furthermore, by combining and overlaying these techniques, the information in the data may be enhanced (Kokalj and Somrak 2019, 2). As of now, there is a lack of explicit guidelines, conventions and frameworks for the visualization of aerial thermography data. Studies applying aerial thermography for surveys utilize various visualization techniques in their analysis (McLeester *et al.* 2018, 454; Hill *et al.* 2020, 11-12; Salgado Carmona *et al.* 2020, 3-4). To assess the effectiveness of visualization techniques on thermal data, I applied several raster-based methods to the thermograms from Halos. I will now shortly describe these techniques.

Histogram equalization, or histogram stretching, is a simple way of enhancing local contrast. This is achieved by spreading out a narrow range of pixel intensity values to obtain a new histogram over the full available range (Lasaponara and Masini 2012, 19-22). By introducing cumulative cut-off points at certain points in the histogram (i.e. <2% and >98%), the noise by outlying intensity values can be further reduced. Often used in combination with histogram equalization is colour coding. Here, different colour ramps are assigned to the histogram to help instinctively visualize divergent patterns – like hot and cold – in the data.

Difference maps are a way of detecting subtle variations in thermal data by calculating the temperature difference between thermograms of the same area which have been recorded at different times (Hill *et al.* 2020, 11-12). This technique will be applied to identify anomalous patterns across related images in the same area (across one night, for example). Furthermore, thermal anomalies can potentially be distinguished by performing time series analysis: comparing sequential thermograms of the same area. Danese *et al.* (2010) proposed a method in which the standard deviation across sequential thermograms is calculated for each pixel. On the resulting visualization, a cluster of pixels with significantly less or more variance than neighbouring pixels would indicate the presence of a subsurface material with higher or lower thermal inertia (Danese *et al.* 2010, 484). For my data, I applied this method to the surveys of site B, as here there are more sequential thermograms to analyse.

Principal Component Analysis (PCA) is a method of reducing the dimensionality of the data by condensing the information of a large set of variables into a smaller set, with the least amount of information loss (Lasaponara and Masini 2012, 35-38; Dumoulin 2017, 243-244). It does this by exploring the correlation between variables and providing a new set of least correlated variables. This technique, often applied in multi- and hyperspectral imaging, was applied to sequential thermograms of the same area. This method has the potential to help distinguish anomalies across time-series data. For a more in-depth look into the mathematics of this technique, it is recommended to read Lasaponara and Masini (2012, 35-38). Similar to the standard deviation method, this technique will be applied to flights covering site B.

To investigate how changes in micro-relief can influence thermal signals, several other visualization techniques were applied to the DEM. These were applied using the Relief Visualization Toolbox (Kokalj and Hesse 2017). The most straightforward of these is analytical multi-directional hillshading. By illuminating the surface with multiple artificial suns from various angles, variations in small relief can be distinguishable (Kokalj and Hesse 2017, 16-17). Another visualization method for the DEM is local dominance (LD). This describes per pixel how 'dominant', or tall, an observer would be standing on that point (Kokalj and Hesse 2017, 25).

Data fusion, often referred to as 'blending', describes how multiple image layers, stacked on top of one another, are blended together by a GIS and combined into one combined visualization (Kalayci 2015, 72; Kokalj and Somrak 2019, 10-14). This fusion can be applied to any combination of the previous techniques to emphasize certain features in the images.

In this research, the effectiveness of these techniques is judged on how well they improved the detection and interpretation of thermal anomalies of possible archaeological origin at the Early Iron Age site of Halos.

Chapter 4: Results

In this chapter, I present the results of the analysis. I analysed nine of the conducted surveys at sites B and C of the Voulokaliva plain in Halos (table 2). First, the thermograms will be discussed in terms of the main findings and the visibility of thermal anomalies. Secondly, the anomalies discovered on the thermograms will be interpreted and compared based on the expected signals of archaeology in the area to identify how conditions during data capture affect thermal signals. Thirdly, the applied visualization techniques will be evaluated in their ability to aid in the detection of thermal anomalies.

Starting time of flight	Day	Location	Altitude (in metres)	Average air temperature at time of flight (in °C)	Average day-time air temperature (in °C)	Average night-time air temperature (in °C)	Relative humidity (in percentage)	Recent Precipitation conditions*	Light Conditions	Average Ground Sampling Distance (in cm)
20:55	6-7-2019	Test site B	100	28	37	19	53	None, slight rainfall the night before	After sunset, clear sky	12.52
05:23	7-7-2019	Test site B	100	20	37	19	67	None	Before sunrise, clear sky	13.33
19:58	7-7-2019	Test site B	100	31	34	19	42	None	After sunset, clear sky	5.75
06:24	8-7-2019	Test site B	100	22	34	20	56	None	After sunrise clear sky	4.44
01:36	9-7-2019	Test site B	100	24	37	21	68	None	Before sunrise, clear sky	2.88
20:58	9-7-2019	Test site B	100	28	34	21	69	None	After sunset, lightly clouded	3.90
05:35	10-7-2019	Test site B	100	26	34	22	63	None	Before sunrise, clear sky	8.97
06:00	10-7-2019	Test site C	50	25	34	22	56	None	Before sunrise, clear sky	1.87
21:24	10-7-2019	Test site C	100	28	34	22	73	Slight rainfall in early afternoon	After sunset, moderately clouded	3.01

*Table 2: Overview of the analysed flights, with associated environmental variables and GSD. *Note that more accurate precipitation measurements were not acquired*

4.1 General findings

After processing the thermograms, various anomalies became visible in the two sites (for an overview of all thermograms, see appendices 2 & 3). A rundown of the anomalies at each individual site will now be provided. How these anomalies discovered in the field compared to their hypothesised signals will be discussed in the following section.
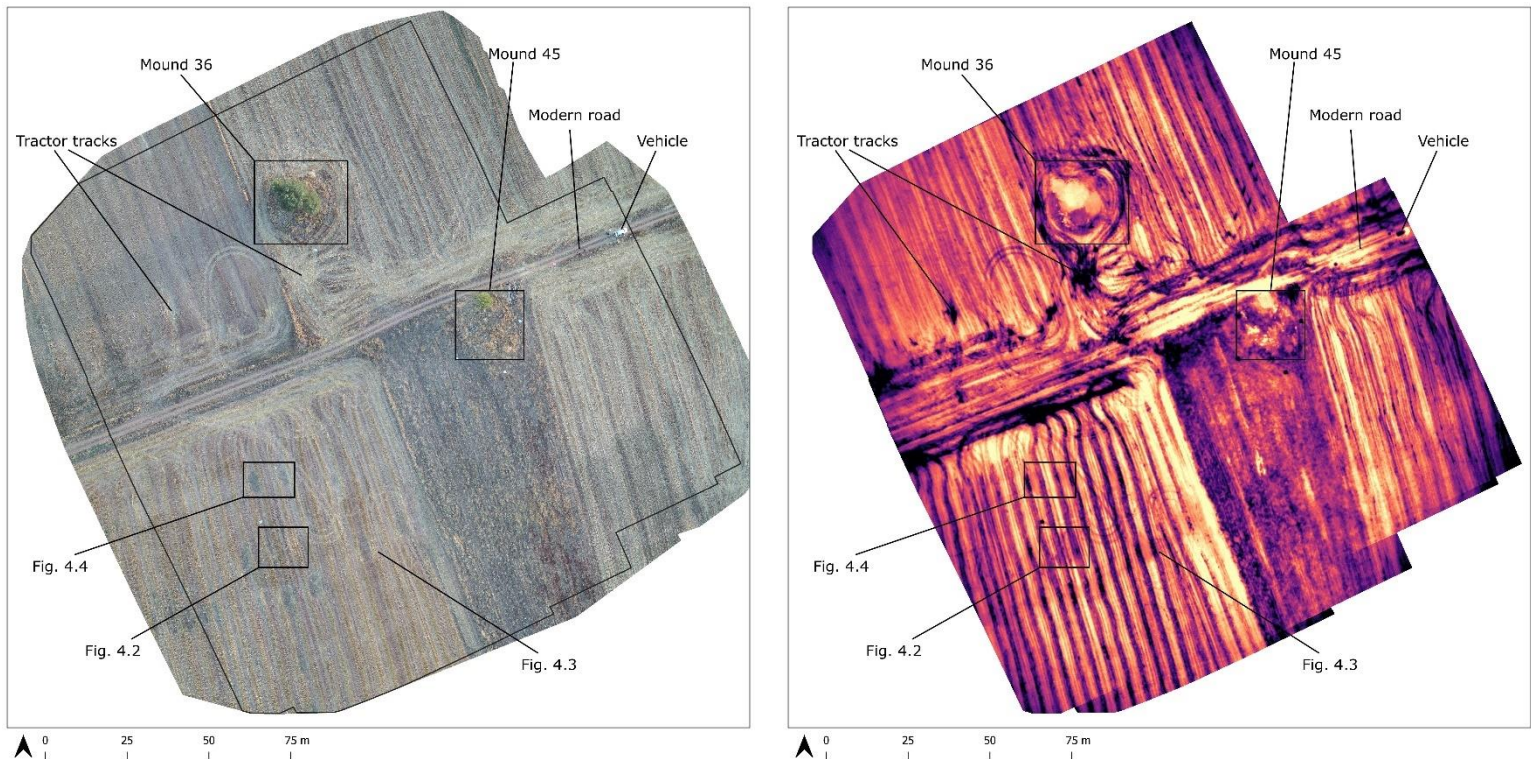

Figure 4.1: An overview of the features on site B. Shown are the optical orthoimage and thermogram of the flight of 06:24 a.m. on the 8th of July. Darker colours denote cooler areas, lighter colours denote warmer areas on the thermogram.

First, the anomalies of site B are introduced (fig. 4.1). In all thermal images of site B, the modern dirt road, the rows of harvested crops, and the vehicle of the survey team appeared very clearly. There was quite a lot of thermal noise present due to the tracks of agricultural vehicles, which have caused areas of vegetation on the surface to become compacted.

Several anomalies related to archaeological features were also present. Mounds 36 and 45, known tumuli with prominent topographical expressions in the landscape, appeared distinctly on the thermograms. Additionally, an oval-shaped thermal anomaly was discovered on the southwest field (fig. 4.2). On the thermograms, this feature remained slightly cooler than the surrounding soil during the night and pre-dawn images. It has a

36

slight expression in the relief, which is highlighted on the flights around sunrise. The feature hardly shows on the optical images but does have an expression on the DEM. It measured 8.2 meters and 4.1 meters at its longest and widest points respectively and showed a roughly 20-centimetre height difference to the surrounding ground. Due to its relative shape, size, and expression in the relief, this feature most likely corresponds to Mound 44. This is a tumulus which during the 1990 survey was much more discernible and had scatters of sherds on the surface (Stissi 2004, 96-98). This deterioration of this feature showcases the ongoing destruction of archaeological features at Halos, as it seems probable that this mound was further damaged by mechanical tillage.

0   5   10   15 m
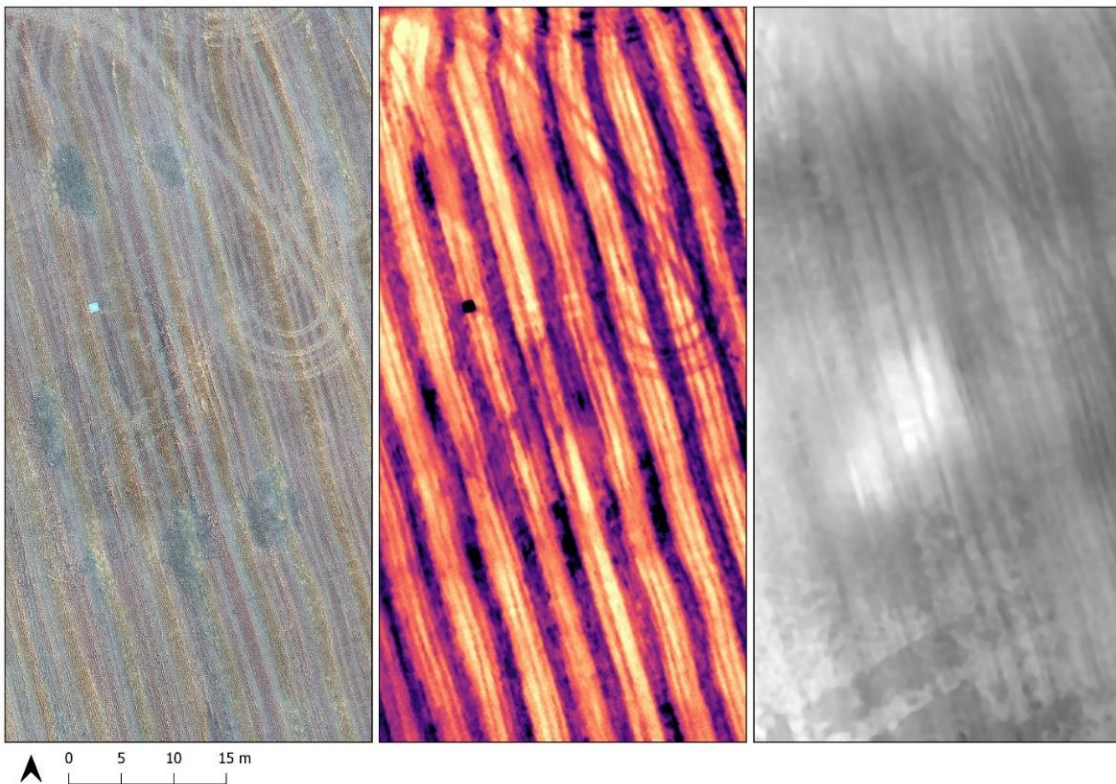
Figure 4.2: Side-by-side view of the optical ortho-image, thermogram, and digital elevation model for the possible Mound 44 on site B. Darker colours denote cooler areas, lighter colours denote warmer areas on the thermogram.
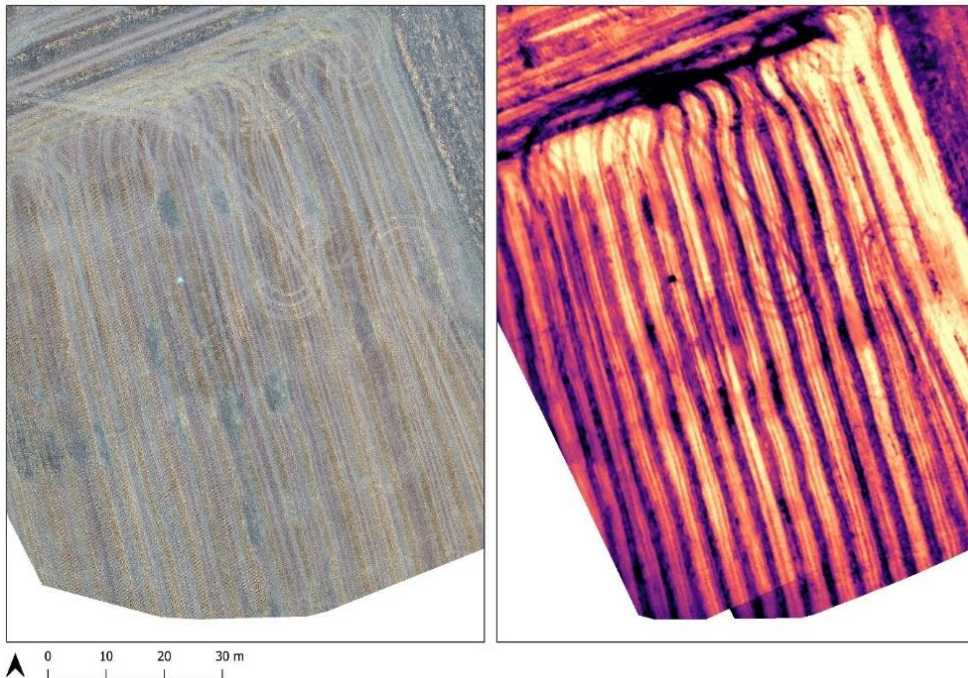
Figure 4.3: Side-by-side view of the optical ortho-image and the thermogram for the elongated cool feature on site B. Note that several of these parallel lines are visible in the optical ortho-image. Darker colours denote cooler areas, lighter colours denote warmer areas on the thermogram.

In the same field as the probable Mound 44, several elongated anomalies with cool thermal signatures were present on the thermal imagery. The largest ones of these stretch itself across the entirety of the field in an east-west orientation (fig. 4.3, above). In several places on these features, cooler anomalies are present (fig. 4.4, below). On the optical imagery, these likely moisture-retaining features coincide with positive crop marks. The location of these anomalies is striking, as at first glance these seem to be surrounding the tumulus. However, due to their large size, with the smallest of these anomalies being more than 3 meters in length, these features most likely do not correspond with subsurface archaeology like the previously discussed single graves. Rather, these anomalies together point to the remains of a now long-eroded stream bed. This also explains the low-value thermal signals, as these areas have been filled in with eroded soils that now preferentially retain water.
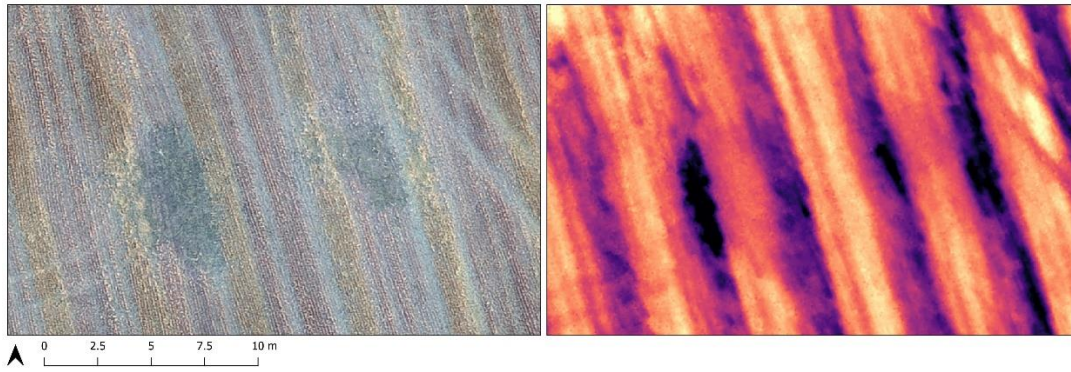
Figure 4.4: Side-by-side view of the optical ortho-image and thermogram of two of the many cool anomalies on site B discussed in the text. Darker colours denote cooler areas, lighter colours denote warmer areas on the thermogram.
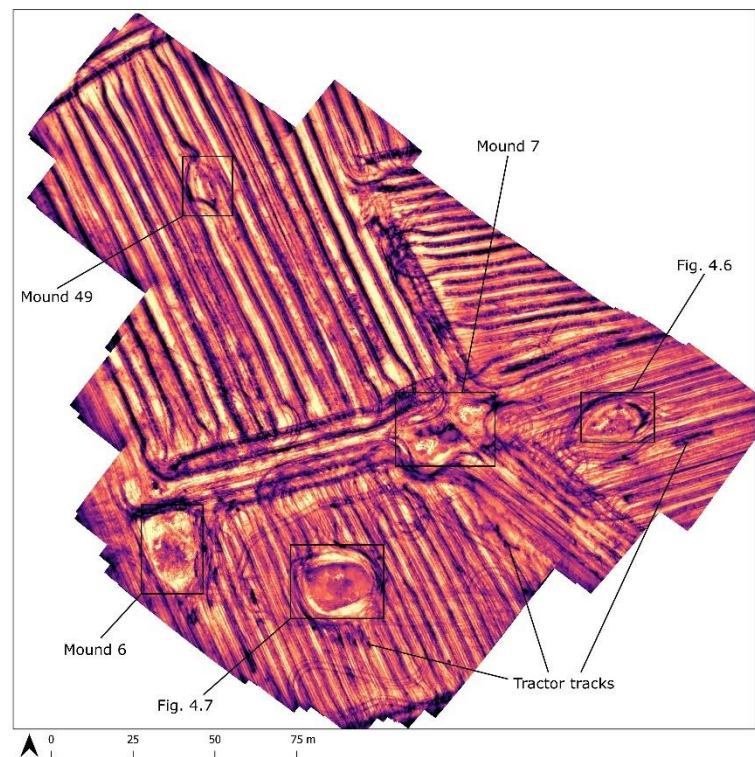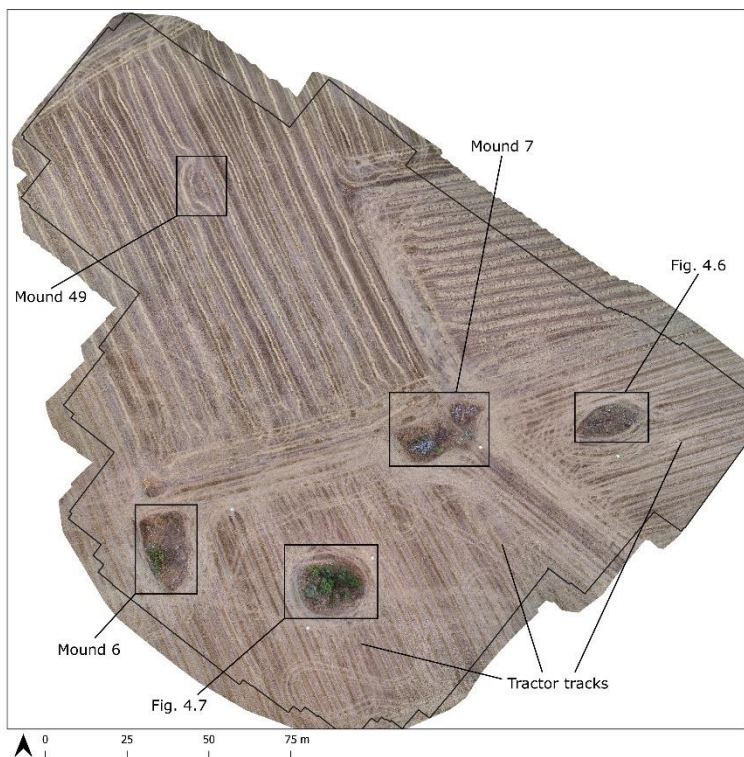

Figure 4.5: An overview of the features on site C. Shown are the optical orthoimage and thermogram of the flight of 06:00 a.m. on the 10th of July. Darker colours denote cooler areas, lighter colours denote warmer areas on the thermogram.

Now, the anomalies at site C are examined (fig. 4.5). Within the extent of this survey area, three damaged and two relatively intact tumuli are present. The three damaged tumuli - Mounds 7, 48, and 49 – were all distinctly visible in the thermal images. Like many of the tumuli in Halos, their tops were covered with scatters of pebbles and cobbles (fig. 4.6, below). The patterning in the pebbles on Mound 48 is most likely caused by the manual casting aside of stones found in the agricultural field onto the tumulus. What is more interesting, is that the cooler areas on the thermal image do not all appear to be directly related to the vegetation. It could be possible that this is caused

by variations in microrelief: low-lying parts of the tumulus preferentially retaining water and therefore showing low temperatures on the thermogram. Evidence for this hypothesis could however not be deduced from the resolution of the elevation model.
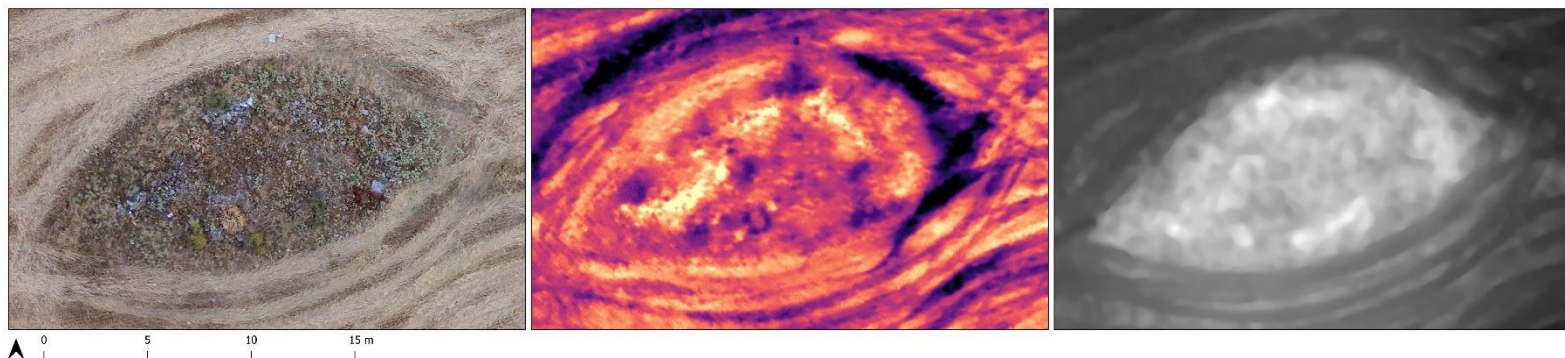

Figure 4.6: Side-by side view of the optical ortho-image and the thermogram showing a concentration of surface artefacts on site C's Mound 48. Darker colours denote cooler areas, lighter colours denote warmer areas on the thermogram.

From the thermograms of the intact tumuli, Mound 5 and Mound 6, more information could be extracted. The tops of these tumuli are largely covered in vegetation. However, between the active vegetation on Mound 5, the largest tumulus in this area, a relatively cool signal could be ascertained (fig. 4.7, below). On the ortho-image and digital elevation model, this cool signal is related to a slight depression on the top of the mound. This crater could be evidence of illegal looting activities, which have already frequently taken place on these mounds (Reinders *et al*. 1991, 31; Stissi 2004, 98). Additionally, the parts of Mound 5 not covered by vegetation show very strong warm signals on the thermal images. This will be examined in the next section.
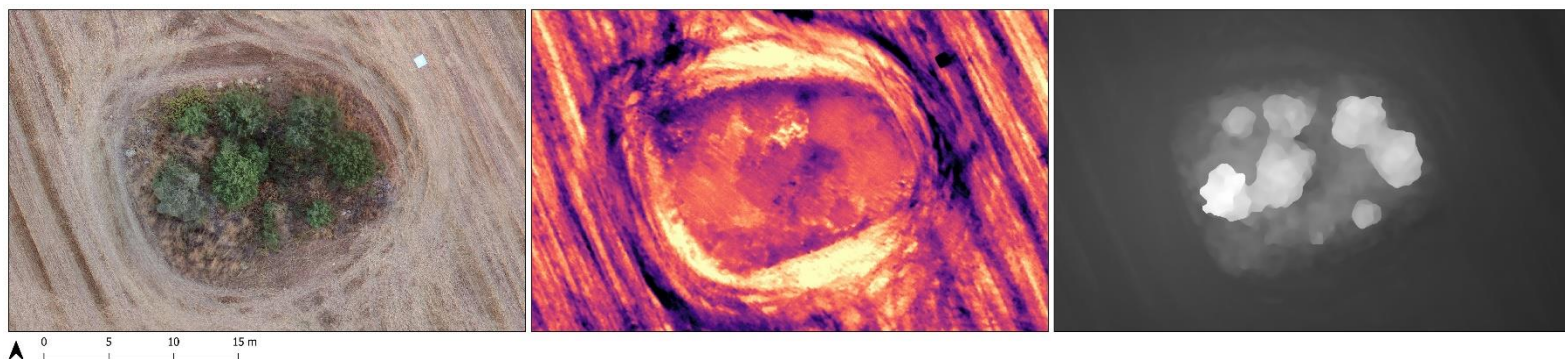

Figure 4.7: Side-by-side view of the optical ortho-image, thermogram, and digital elevation model for Mound 5 on site C. Darker colours denote cooler areas, lighter colours denote warmer areas on the thermogram.

Thermal anomalies which could be interpreted as single graves were not present in either of the surveyed sites. This observation will be discussed in-depth in the discussion.

40

Besides the anomalies at sites B and C, several other observations could be made on the thermal imagery. In general, the thermograms at 100 meters altitude were of a sufficiently high resolution to discern small features in the landscape, such as surface scatterings of pebbles and loose cobbles. In two cases, namely the flight at 20:55 on the 6th and the flight at 05:23 on the 7th of July, the resolution was of poor quality. This was most likely caused by the low amount of images taken during these surveys. At site C, the two flights conducted on the 10th of July were flown at different altitudes: the 06:00 flight at 50 meters, and the 21:24 flight at 100m meters. The lower altitude survey did provide an improvement in the average ground sampling distance, albeit only a minor one (1.87 cm versus 3.01 cm). Several thermal anomalies were discovered in the images. These will be discussed in-depth in the next part of this chapter.

There was a significant variation in the thermal visibility of the images. Figure 4.8 (below) shows six thermograms of the same portion of site B recorded across several days at different times.
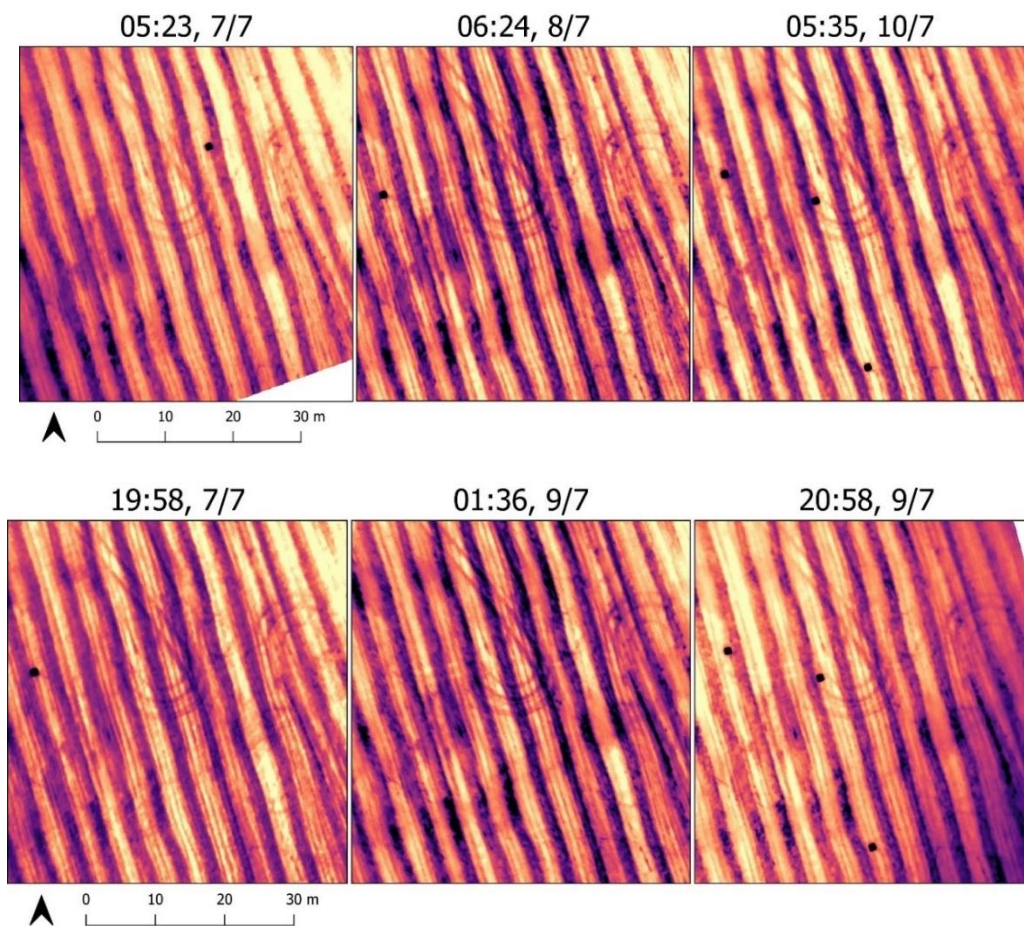

Figure 4.8: A comparison of several thermograms of the same area across surveys at 100m altitude. The top row shows thermal images taken in the morning. The bottom row shows thermal images taken in the evening. Darker colours denote cooler areas, lighter colours denote warmer areas.

41

The flights which took place just before sunset provided images with muted thermal contrasts (fig. 4.8, top left; top right). After an entire night of cooling, differences in thermal inertia were minimised, leading to relatively uniform thermal signals. The flight which took place right after the sun came up, at 06:24 on the 8th of July provided better visibility (fig. 4.8, top centre). With the warming of the soil, the different features and materials on the surface start to heat at different rates due to differences in thermal inertia. Also, the oblique angle of the sun at dawn highlighted features with a topographical expression. The flights just after dusk generally provided images with stronger thermal contrasts and relatively good visibility (fig. 4.8, bottom left; bottom right). On the whole, the flight of 01:36 on the 9th of July provided the best visibility of thermal anomalies on site B (fig. 4.8, bottom centre). As a result of a few hours of cooling, the differences in thermal inertia between features on the surface were recognizably distinct.

All flights were performed at moments with moderate to moderate-high relative humidity. Air saturated with moisture can, as previously stated, act as a 'thermal blanket'. This means it was possible that recorded thermal signatures of objects were weakened, however, the impact of this is not readily apparent. Interestingly for the flights at site C, an instance of transient heat flux was recorded. In the afternoon of the 10th of July, between the flight of 06:00 and 21:24, a small moment of rain occurred. This was the first rain since the 5th of July. When comparing the resulting thermograms of these flights, no immediate change in the visibility of thermal anomalies became apparent.

4.2 Thermal anomalies and the evaluation of expected thermal signals

In chapter 3.2.1, the hypotheses were formulated of the thermal signals of expected archaeological features. These hypothesised signals were used in the process of identifying thermal anomalies and assessing the impact of environmental factors in the field. What follows now is a comparison between the anomalies encountered on the thermograms and the hypothesised signals. At the end of the chapter is a table containing the results of this comparison in a more easily digestible format (table 3, below).

Mound 36, site B

Mound 6, site C

Mound 45, site B

Mound 7, site C

Mound 5, site C

Mound 48, site C

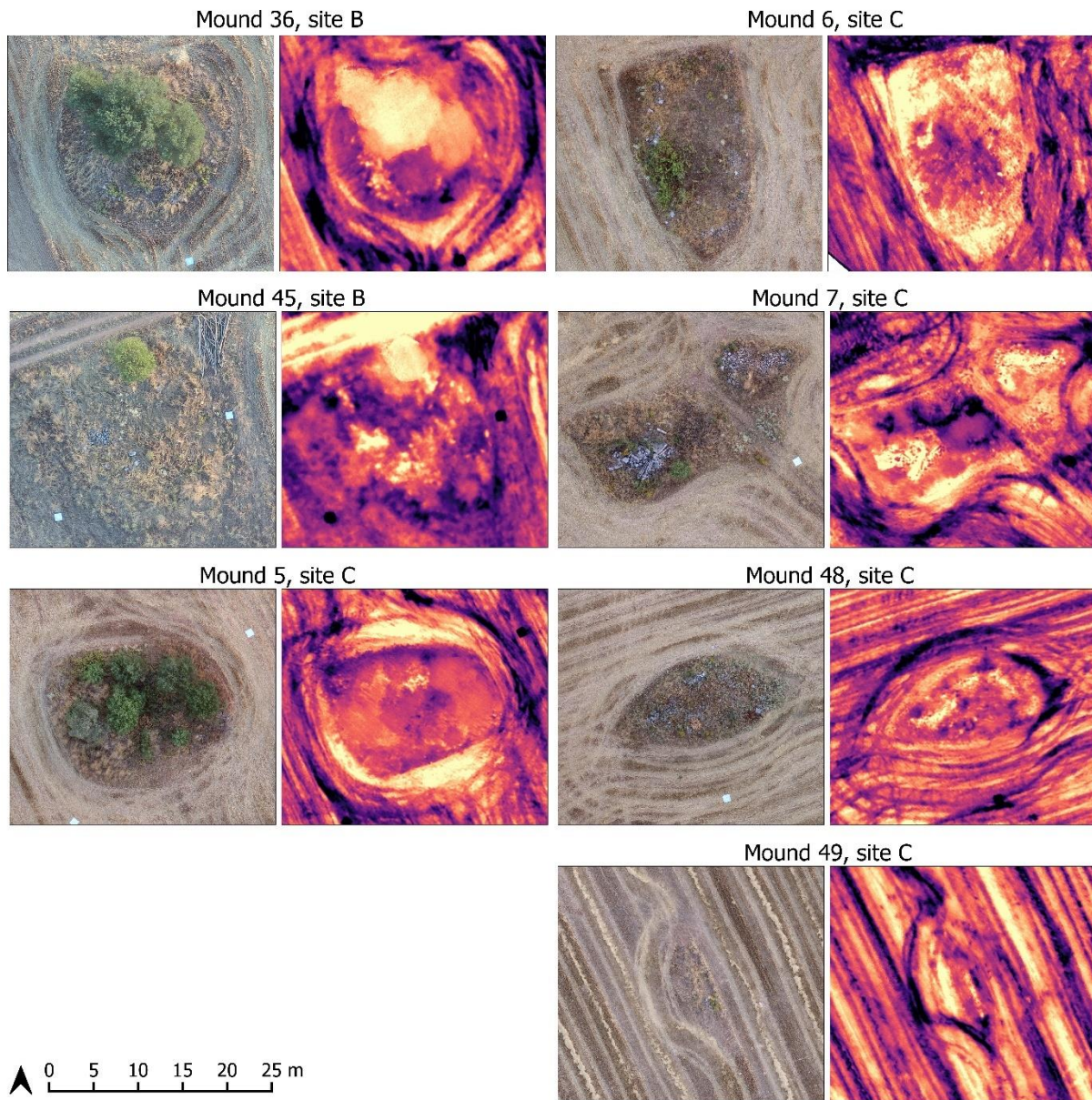Mound 49, site C

0 5 10 15 20 25 m

Figure 4.9: An overview of the mounds at both site B and site C. For each mound, the associated optical and thermal images are shown. Darker colours denote cooler areas, lighter colours denote warmer areas on the thermogram.

Figure 4.9 provides an overview of the tumuli in site B and site C. These features, first identified in the field surveys in 1990, displayed thermal anomalies which were mostly consistent with their hypothesised thermal signatures described in this thesis. The thermal signature of the mounds consists of several attributes.

On the vertical angle of the thermograms, the active vegetation on the tops of the mounds is immediately discernible. The temperature of vegetation is controlled by plant transpiration (Périsset and Tabbagh 1981, 169). This entails that the trees and large shrubs act as a screen which filters the thermal-infrared response of the mound below

43

it. In my hypothesis, I underestimated the impact vegetation would have on the thermal signal of the tumuli. The parts of some of the mounds not covered by vegetation show very strong warm signals (fig. 4.9, especially visible on Mound 5, Mound 6). In my formulated hypothesis, I expected the remnants of the layers of cobbles and pebbles originally covering these features to be visible beneath the soil as a large warm thermal signal. The strong warm signals of the bare soil of the tumuli somewhat match this hypothesis. Another expectation was that the raised position in the landscape of many of these tumuli would cause differential heating and cooling due to oblique insolation. This expectation did indeed come to pass, as has been explored with the highlighting of the probable Mound 44.

As for the hypothesised thermal signal of the single graves, no direct comparison can be performed. No anomalies pointing to the presence of single graves in sites B and C were discovered. This absence is striking, and the reasons for this will be explored more in-depth in the discussion (chapter 5).

The thermal signal of the surface scatters had been formulated as concentrations of small warm signals. On the thermal images, it became clear that all scatters on the sites consisted of pebbles, cobbles and fragments of slabs. These stones possess noticeably distinct characteristics, such as higher volumetric heat capacity, which differentiated them strongly as warm anomalies on the thermal images. What was unexpected about these signals however, was their location in the sites. These features were *only* found on the tops of the tumuli, with no scatters appearing in any of the agricultural fields themselves.

Archaeological feature	Hypothesised thermal signal	Thermal signal in reality
Tumuli	• Stone cover is visible as a **large warm thermal signal**, internal structure beneath this cover will be masked. • If the tumulus has a topographic expression, the exposed side will show a **high thermal signal** due to oblique insolation.	• Bare soil around tumulus shows a **very warm thermal signal**. • Topographic expression shows a **high thermal signal** on the exposed side. • Vegetation adds thermal noise as **cool signals**.
Single graves	• If the graves are close enough to the surface and are not damaged: **visible as warm areas**. (These could be masked by subsurface inclusions). • If the graves are located deeper or significantly damaged: **not visible on the thermograms.**	• **Not visible on the thermograms** (see chapter 5 for the interpretation of this absence)
Surface scatters	• Visible as **concentrations of small warm signals.**	• Visible as **concentrations of small warm signals** only located on tumuli.

Table 3: A summary of expected archaeological features at the site of Halos and their hypothesised signal on the thermal images, contrasted with thermal anomalies discovered in the field.

4.3 Evaluation of the visualization techniques

The raster-based visualization techniques outlined in chapter 3 were applied to the thermal datasets. In this part, these techniques are evaluated by their ability to aid in the detection of thermal signals of anomalies at the site.
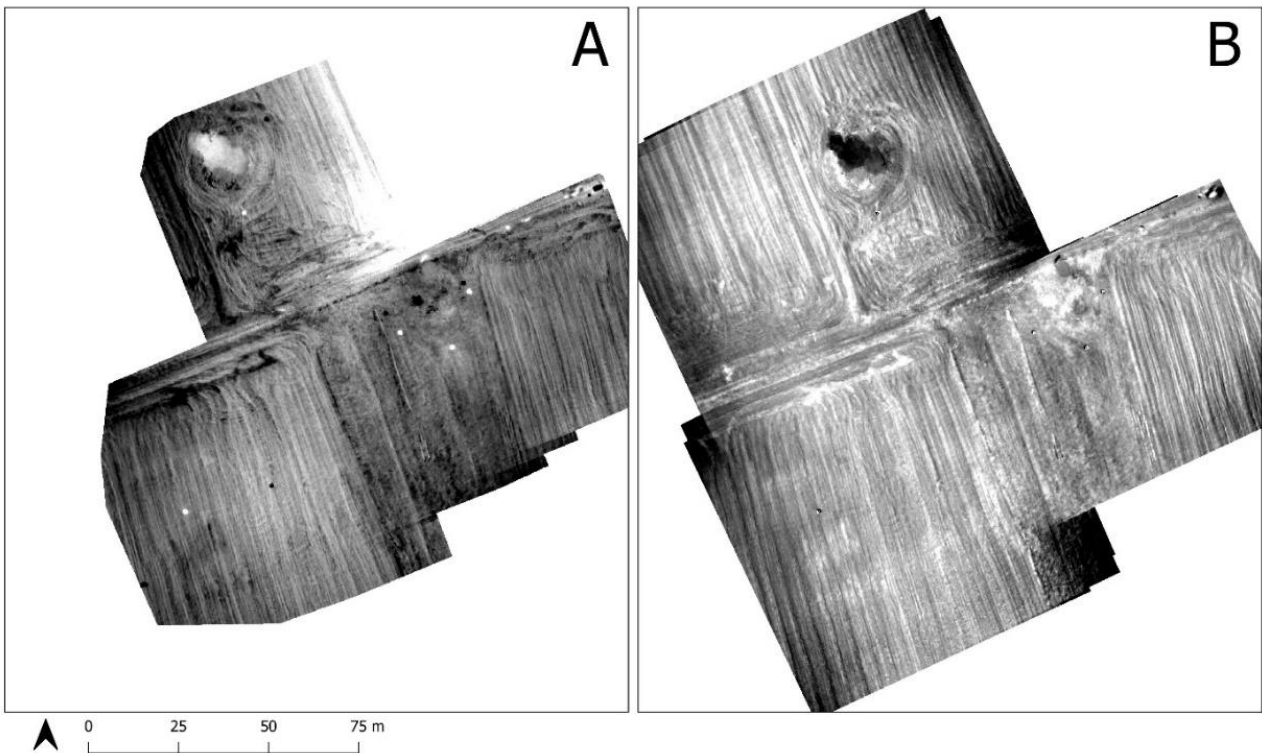

Figure 4.10: Two examples of difference maps of site B: (A): shows the difference between the early morning flight of 05:23 on 07/07 and the evening flight of 19:58 on 07/07. (B): shows the difference between the evening flight of 19:58 on 07/07 and the following morning flight at 06:24 on 08/08.

Difference maps were created to visualize how the emission of thermal infrared radiation changes across certain time periods, such as across one night or day. In practice, this method turned out to be a quick and easy method for highlighting anomalies. The best results were obtained by calculating the difference between flights after sunset and around dawn (fig. 4.10). This method increased the contrast of the ploughed Mound 44 and the moisture-retaining features. The standard deviation map, while helpful in emphasizing the differences in thermal inertia of features in sequential thermograms, did not provide any better results than the difference maps (fig. 4.11, A; below).
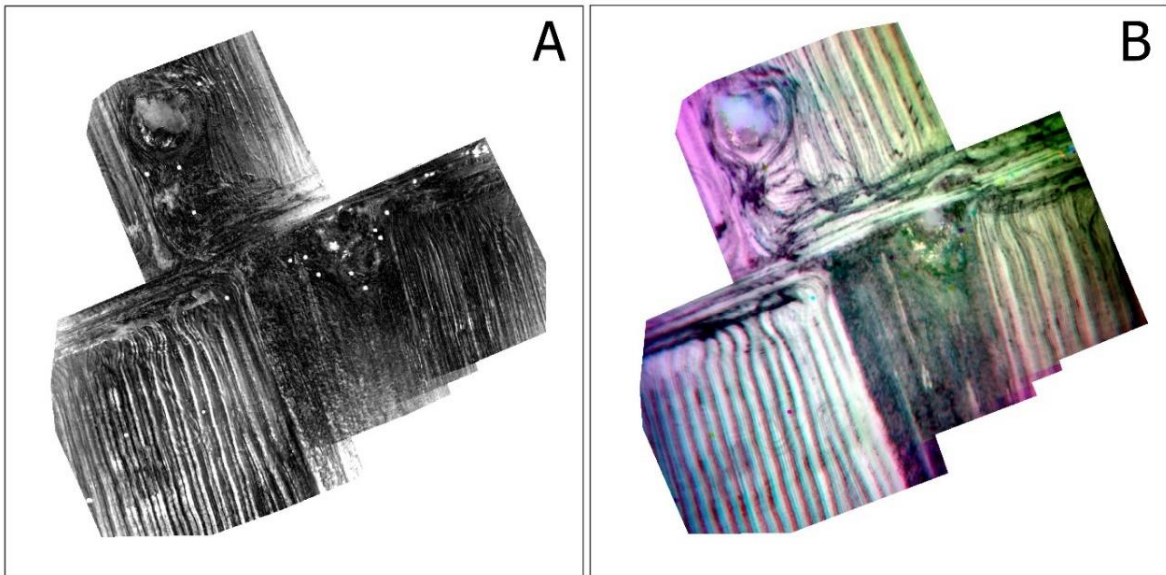
Figure 4.11: (A): The standard deviation map of site B. (B): The first three principal components of site B visualized as an RGB composite.

In this research, the principal component analysis provided the clearest detection of anomalies in the data (fig. 4.11, B). This visualization shows the first three principal components as RGB raster bands. This method provided increased visibility of all previously described signals. This method was not applied to the surveys of site C, as two flights were too little to meaningfully assess the result of a principal component analysis on the area. Applying data fusion helped exaggerate some of the features, but was ultimately not helpful in providing many new insights on the data of Halos. For instance, by overlaying the Local Dominance map with the thermograms of site B, the impact of differences in microrelief on thermal signals was visualized (fig. 4.12).
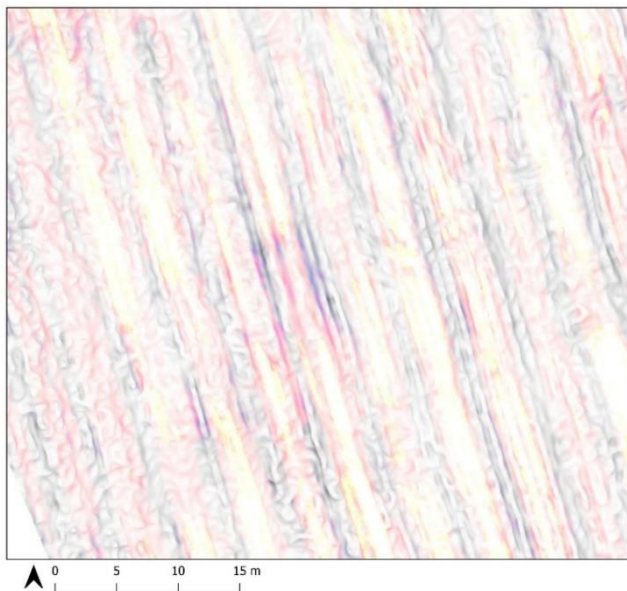
Figure 4.12: This detail of the possible mound 44 on site B shows the Local Dominance overlaid with the thermal data using the 'lighten' blend method. The purple region shows a cool, higher-lying expression in the relief.

Chapter 5: Discussion

The goal of this thesis was to identify how drone-based thermal imaging methods during data capture and data visualization could aid in the detection of archaeological features at the site of Halos. In this chapter, my results are connected to the existing body of knowledge relating to the archaeology of Halos and the practice of aerial thermography. In addition, my methods and results are critically examined. It should be noted that the thermal surveys at Halos are an ongoing research project, and the results of this thesis will help contribute to the future strategy of surveys at the site.

The ability of drone-based thermal imaging to detect scatters of surface artefacts is a minor, yet interesting quality of this technique. Previous research using handheld thermal cameras has demonstrated that minute concentrations of obsidian can be detected using this technique (Buck *et al.* 2003, 988-989). In this research, similar results were demonstrated with scatters of cobbles and slabs, originally from these tumuli. Concentrations of these features offer interpretations based on their form, distribution and context. Furthermore, being able to remotely sense these features offers new possibilities for aerial thermography to be used in conjunction with pedestrian survey. This is especially helpful in the Mediterranean, where fieldwalking is often limited to agricultural land and it sometimes occurs that access is denied to certain fields (Campana 2018, 11-13; 44-50). Here, aerial thermography provides a quick, cheap, and non-invasive method of mapping surface distributions.

The single graves, discovered only in the excavation of the national highway and missed in all other surveys, provided an interesting case study for the potential of aerial thermography. However, no evidence pointing to the presence of single graves was discovered at sites B and C of the Voulokaliva plain. This could suggest several things. In the excavation of the national highway, only a narrow stretch of land was investigated, meaning the total boundaries of this cemetery have not yet been clarified (Tsiouka 2008, 6). The absence of these features in the thermal survey could mean the extent of the single graves did not reach this far north. An argument against this is that these single graves were interspersed with tumuli, more of which were discovered during the excavation (Stissi 2011, 152). The lack of discovered single graves could also have to do with amount of unremitting agricultural activity that has taken place in the surveyed areas. It is a possibility that there is no longer any trace of subsurface archaeological

features like the single graves. The problem with this notion, is that the single graves discovered in the highway excavation were also located on deep-ploughed fields (Tsiouka 2008, 12). Furthermore, even if these features were ploughed away, the graves would leave a sherd and stone scatter. These were not discovered in the field, making this option unlikely. Another suggestion is that single graves were present in the surveyed area, but the aerial thermography survey was not able to sense them. The most obvious reason for this, is the soil at the site. In experiments by Cool it was found that a surface ground cover consisting only of clay soil obstructs all thermal signals beneath it (2015, 50). Similarly at Halos, the poorly conductive sandy-clay soil and the inactive vegetation on the surface ground cover severely impeded the amount of thermal infrared radiation which could penetrate to the depth of potential subsurface features, thus limiting the effectiveness of thermography to sense anomalies beneath the ground.

While the visibility of subsurface anomalies was found to be lacking, this research has shown that aerial thermography is able to remotely sense mostly destroyed tumuli. Previous research into airborne thermography similarly demonstrated this quality (Giardino and Haley 2007, 69-71). While this ability is interesting, the added value of thermography has to be compared to established methods. Mound 44 was mostly detected due to its expression in the landscape which, while minor, caused differential heating and cooling. There is an already longstanding tradition of detecting burial mounds using airborne laser scanning techniques such as LiDAR (Chase *et al*. 2017, 94-97). One of the main benefits of using LiDAR for this purpose is its ability to sense features of interest through a vegetation cover (Risbøl and Gustavsen 2018, 333-337). However, in this research, LiDAR data was not available. The data sources that were available at Halos, were the optical ortho-images and the thermograms. Here, the thermograms did provide additional benefits over solely using the optical imagery, as nearly imperceptible relief expressions and distributions of surface artefacts were easily distinguished on the thermal images.

The question remains if aerial thermography is capable of sensing these mounds if there is no remaining relief expression. This research does not provide evidence for this fact. Recently, the application of magnetometry, a geophysical technique, has shown its prowess in detecting several completely levelled mounds in Iowa, the United States

(Green *et al.* 2021, 306). This magnetic survey, even with a motorized platform, took two weeks to cover an area of 0,086 km^2. If it is found that aerial thermography can similarly sense mounds with no trace in the landscape, drone-based thermal imaging would offer a much faster and cheaper alternative to cover such an area. This would especially be the case if the variables dictating the optimal moment of capture for aerial thermography are completely understood.

In this regard, my research contributes useful insights to the understanding of how to get the most out of drone-based thermography surveys . Currently, the issue of optimal flight timing remains unresolved. At Halos, it was found that the optimal time to apply thermal imaging is at night. This is in line with the prevailing sentiment, as several case studies have shown similar results (Cool 2015, 78; Casana *et al.* 2020, 770; Hill *et al.* 2020, 9). At this time, the diurnal heat flux has changed to negative, and features will have had a few hours to cool, exposing differences in thermal inertia. The previously mentioned survey at Villasviejas, Spain, counter-intuitively showed the optimal moment for data collection to be around noon (Salgado Carmona *et al*. 2020, 9). This hypothesis cannot be tested in this thesis, as none of the conducted flights at Halos took place around that time.

The importance of microrelief as a factor in highlighting thermal anomalies has already been discussed in the work of Scollar *et al*. (1990, 601). In their work, flights between the early morning and noon were posed to strengthen these patterns. The results of the thermal survey at Halos corroborate this fact. Morning flights, just after sunrise, demonstrated their effectiveness in highlighting differences in topography at the site, leading to the (re)discovery of the previously discussed Mound 44. Combined with the improvement in visibility of thermal contrasts (see section 4.1), flying just after the sun comes up can provide high-quality thermal images.

Transient heat flux is another factor that has been shown to influence the results of a thermal survey. In this research, the flights hours before and after the rain event at site C provide an interesting insight into this factor. It has been demonstrated that the ideal window for collecting thermal data after an instance of transient flux is very narrow, possibly only a day (Cool 2015, 79). No substantial difference in the visibility of thermal anomalies was perceived at Halos. Possibly, the amplitude of the transient flux was not

large enough to cause a noticeable change, as it had only been a few days since the last rainfall. It is however difficult to come to a considered decision on this fact as the archaeological visibility was already lacking due to the previously stated factors. For future surveys, however, care needs to be taken in finding the appropriate moment by paying close attention to local climatic and meteorological conditions.

Regarding the visualisation techniques which were applied in the analysis, the main objective of these was to expose patterns in time-series data. Especially the PCA, which could condense the results of several flights into one image was a productive tool in identifying thermal anomalies. Areas which show stark changes in temperature across a period can also point to the of anomalies, and the simplest, and remarkably helpful, method in displaying this is by constructing difference maps.

During the analysis, however, some of the limitations with the current strategy of thermal surveys at the site came to light. The first and foremost of these is the fact that there has been no validation in the field of the anomalies that were discovered in the analysis. The surveys took place over areas that have for the most part not been archaeologically excavated, and there are currently no plans in the upcoming field season for site B and C to be investigated. In the next campaign, a part of Magoúla Plataniótiki will be investigated. It would be interesting to see aerial thermography be applied to an area which is under excavation to provide field validation to the survey results. Another limitation is that aerial thermography and visible light photography were the only methods of remote sensing applied at Halos. Many other studies applying aerial thermography also make use of additional techniques, such as multispectral imaging, magnetic survey, or ground-penetrating radar. By using multiple distinct remote sensing methods, the results of each technique can be cross-referenced and possibly provide more information than the sum of individual techniques through the means of data fusion (Kalayci 2015). In regards to the analysis, the different extents of each flight meant only some parts of the site were covered in multiple surveys. This excluded several areas of the site from the quantitative methods. However, as a drone is used in this survey, this issue can be easily resolved by establishing the same pre-defined autonomous flight paths for all flights over an area. Another factor which had an impact on the comparison between the expected signals and the recorded signal was the fact that the temperatures of the soil were not recorded. Soil temperature is critical in understanding how deeply diurnal and transient heat flux is affecting and reflecting

temperatures at the surface (Hill *et al.* 2020, 17). For future campaigns, the collection of this information is vital in establishing the optimal moment for surveying.

All in all, the results at the site of Halos exhibit the wide range of factors which have a hand in shaping the outcome of a thermal survey. While in general the visibility of potential anomalies relating to archaeology may have been lacking, deeper knowledge was attained regarding the application, optimization, and limitations of aerial thermography.

Chapter 6: Conclusion

In this thesis, I have aimed to answer how drone-based thermography data capture and visualization techniques can best be employed to identify archaeological features at the Early Iron Age funerary landscape of Halos. This multi-period site, spanning from the Early Neolithic to near-modern times, has been the subject of many surveys and investigations, but this drone-based thermal survey had been the first time a remote sensing method was applied to the site. By formulating the hypothetical thermal signatures of possible archaeological features in the area and comparing these to anomalies discovered during the survey, I was able to identify features of interest and evaluate how data capture conditions influenced thermal signals in the field. A qualitative visual assessment was performed of the thermal data. During this assessment, several visualization techniques were applied and evaluated in their ability to aid in the detection of thermal anomalies by highlighting patterns in time-series data.

Several features of archaeological interest were sensed, such as concentrations of surface artefacts and the remains of a mostly eroded burial mound. However, the limited visibility of subsurface anomalies at Halos emphasizes that environmental variables, such as the ground cover, play an important role in the success of a thermal survey. Clay-rich soils and soil reworking are two factors that can, to a great extent, obscure the visibility of subsurface features on the thermograms.

Nevertheless, more insights regarding the optimal timing of surveys and the impact of transient heat flux were gained. At Halos, flights at night provided the greatest thermal contrasts. Also, the rain event on the last day showcased how the magnitude of heat flux is an extremely important factor in the effects of transient heat flux. Thus, with this knowledge, the thermal survey strategy at the site can be enhanced. By planning surveys at night, around optimal moments with a high magnitude of thermal flux, the visibility of possible thermal anomalies will be greatest. This magnitude can be better established by collecting additional data on soil moisture and temperature. Flights at moments with oblique insolation, for example around dawn, can help highlight important differences in microrelief, and should therefore also be performed during surveys. By analysing the thermograms using visualization techniques that highlight patterns of change through time, such as PCA and difference maps, more anomalies can be recognized. However, for the greatest effect of quantitative visualization techniques, a systematic coverage

and identical extent is required between flights covering the same area.

There are several avenues for future research, both into the site of Halos and the application of aerial thermography. Firstly, to build up a knowledge base of field-validated thermal anomalies, it could be useful to apply thermal imaging to areas in Halos which have been or will be archaeologically excavated. This can be done, as mentioned in chapter 5, by thermally surveying the areas under investigation in the upcoming field seasons. Secondly, the effects of seasonal heat flux have not yet been thoroughly examined. It would be interesting to perform more thermal surveys in other seasons, such as in the winter for Halos, and compare the thermograms of multiple seasons. This can certainly be implemented in the ongoing project, as the investigation of Halos is still ongoing. The visualization methods applied in this thesis could similarly be applied in this analysis. Thirdly, more advanced techniques can be tried to identify patterns in multi-temporal thermal data. One such technique, a self-organizing map (SOM), is a promising type of artificial neural network which has already seen use in a small scale analysis of thermal data (Danese *et al.* 2010, 485-488). This is out of the scope of this project, but does provide interesting angles for future research.

The value of thermal imaging as a remote sensing technique will improve once our understanding of the conditions that are conducive to a successful thermal survey is refined. This is done through case studies such as this, which explore the possibilities and limitations of the technique. Aerial thermography has already in many cases proven to be a powerful method of remote sensing, capable of providing archaeologists with results that rival established geophysical methods. In addition, the application of thermal imaging in conjunction with a UAV platform offers archaeologists a quick, operationally flexible, and relatively cost-efficient method for recording high-resolution remote sensing data over a large area. Especially with the use of autonomous flight planning apps, consistent coverage can be achieved across multiple flights with ease.

With the continuous improvements in drone and thermal sensor technology, this method will only become more accessible and productive in the future. Therefore, I foresee aerial thermography becoming an integral part of any archaeological prospection campaign.

Bibliography

Ancient sources

Demosthenes, *On the false Embassy (Oration 19)*. Translated by D.M. MacDowall. Oxford
University Press, 2000.

References

Abrams, M.J. and D.C. Comer, 2013. Multispectral and Hyperspectral Technology and
Archaeological Applications in *Mapping Archaeological Landscapes from Space*. New
York: Springer. 57-71. https://doi.org/10.1007/978-1-4614-6074-9_6

Agnousiotis, D., Dijkstra, T., Efstathiou, D., Heymans, E., Mamloudi, I., Reinders, H.R., Rondiri, V.,
Stamelou, E., and V.V. Stissi, 2020. The 2013-2014 Test-trenches at Halos. *Αρχαιολογικο
Εργο Θεσσαλιασ Και Στερεασ Ελλαδασ* 1, 301–310.

Buck, P.E., Sabol, D.E. and A.R. Gillespie, 2003. Sub-pixel artifact detection using remote sensing.
Journal of Archaeological Science 30(8), 973–989. https://doi.org/10.1016/S0305-
4403(02)00284-4

Campana, S., 2017. Drones in Archaeology. State-of-the-art and Future Perspectives.
Archaeological Prospection, *24*(4), 275–296. https://doi.org/10.1002/arp.1569

Campana, S., 2018. Mapping the Archaeological Continuum. Filling 'Empty' Mediterranean. New
York: Springer. https://doi.org/10.1007/978-3-319-89572-7

Casana, J., Kantner, J., Wiewel, A., and J. Cothren, 2014. Archaeological Aerial Thermography: A
Case
Study at the Chaco-era Blue J Community, New Mexico. *Journal of Archaeological
Science* 45,
207–219. https://doi.org/10.1016/j.jas.2014.02.015

Casana, J., Wiewel, A., Cool, A.C., Hill, A.C., Fisher, K.D. and E.J. Laugier, 2017. Archaeological
Aerial Thermography in Theory and Practice. *Advances in Archaeological Practice*, *5*(4),
310–327. https://doi.org/10.1017/aap.2017.23

Chase A.S.Z., Chase D.Z. and A.F. Chase, 2017. LiDAR for Archaeological Research and the Study
of Historical Landscapes, in Masini, N. and F. Soldovieri (eds.), *Sensing the past:
Geotechnologies and the Environment, vol 16.* New York: Springer.
https://doi.org/10.1007/978-3-319-50518-3_4

Christmann, E. and E. Karimali, 2004. Late Neolithic and Early Bronze Age, in H.R. Reinders (ed.),
Prehistoric Sites at the Almirós and Soúrpi Plains (Thessaly, Greece). Assen: Koninklijke
Van Gorcum, 39-73.

Cool, A.C., 2015. *Aerial Thermography in Archaeological Prospection: Applications & Processing*.
(Master's thesis. University of Arkansas, Fayetteville, USA). Retrieved from
https://scholarworks.uark.edu/etd/1157/

Cool, A.C., 2018. Thermography, in S.L. López Varela (eds.), *The Encyclopedia of Archaeological Sciences*. Hoboken: Wiley. 1-5. https://doi.org/10.1002/9781119188230.saseas0579

Danese, M., U. Demšar, N. Masini, and M. Charlton, 2010. Investigating Material Decay of Historic Buildings Using Visual Analytics with Multi-Temporal Infrared Thermographic Data. *Archaeometry* 52(3), 482–501. https://doi.org/10.1111/j.1475-4754.2009.00485.x

Duffy, J.P. and K. Anderson, 2016. A 21st-century renaissance of kites as platforms for proximal sensing. *Progress in Physical Geography*, 40(2), 352–361. https://doi.org/10.1177/0309133316641810

Dumoulin, J., 2017. Infrared Thermography: From Sensing Principle to Non-destructive Testing Considerations. *Geotechnologies and the Environment*, 233–255. https://doi.org/10.1007/978-3-319-50518-3_11

DJI, 2017. *Matrice 210 Product Specifications.* Retrieved from https://www.dji.com/nl/matrice-200-series/info, accessed on 2 April 2021

DJI, 2018. *Zenmuse XT2 Product Specifications.* Retrieved from https://www.dji.com/nl/zenmusext2/specs, accessed on 2 April 2021

Floras, S. and I. Sgouras, 2004. The Almirós and Soúrpi Plains, in H.R. Reinders (ed.), *Prehistoric Sites at the Almirós and Soúrpi Plains (Thessaly, Greece).* Assen: Koninklijke Van Gorcum, 6-19.

Green, W., Wiewel, A.S. and S.L. De Vore, 2021. Geophysical Detection and Assessment of Leveled Mounds: An Example from the Upper Mississippi Valley. *American Antiquity* 86(2), 1–22. https://doi.org/10.1017/aaq.2020.103

Hill, A.C., 2013. Archaeology and UAVs: Legal, Ethical and Safe Use of Drones for Archaeological Research. *Anthropology News*, 29–30.

Hill, A.C., Laugier, E. and J. Casana, 2020. Archaeological Remote Sensing Using Multi-Temporal, Drone Acquired Thermal and Near Infrared (NIR) Imagery: A Case Study at the Enfield Shaker Village, New Hampshire. *Remote Sensing* 12(4), 1-21. https://doi.org/10.3390/rs12040690

Kalayci T., 2015. Data Integration in Archaeological Prospection, in Sarris A. (Ed.) *Best Practices of GeoInformatic Technologies for the Mapping of Archaeolandscapes*. Oxford: Archaeopress, 71-83.

Kokalj, Ž. and R. Hesse, 2017. Airborne Laser Scanning Raster Data Visualization. A Guide to Good Practice. *Prostor, Kraj, Čas* 14(5). 1-90. https://doi.org/10.3986/9789612549848

Kokalj, Ž. and M. Somrak, 2019. Why not a single image? Combining visualizations to facilitate fieldwork and on-screen mapping. *Remote Sensing* 11(7). https://doi.org/10.3390/rs11070747

Kuenzer, C., and S. Dech, 2013. Theoretical Background of Thermal Infrared Remote Sensing, in Kuenzer C. and S. Dech (eds.), *Thermal Infrared Remote Sensing: Sensors, Methods, Applications.* https://doi.org/10.1007/978-94-007-6639-6

Lagia, A., Papathanasiou, A., Malakasioti, Z., and F. Tsiouka, 2013. Cremations of the Early Iron Age from Mound 36 at Voulokalyva (ancient Halos) in Thessaly, in Lochner M. and F. Ruppenstein (eds.), *Brandbestattungen von der mittleren Donau bis zur Ägäis zwischen 1300 und 750 v. Chr.* 197–220. http://www.jstor.org/stable/j.ctv8d5tfn.16

Lambers, K., 2018. Airborne and Spaceborne Remote Sensing and Digital Image Analysis in Archaeology, in C. Siart *et al.* (eds.), *Digital Geoarchaeology, Natural Science in Archaeology*, https://doi.org/10.1007/978-3-319-25316-9_7

Lasaponara, R., and N. Masini, 2011. Satellite remote sensing in archaeology: Past, present and future perspectives. *Journal of Archaeological Science* 38(9), 1995–2002. https://doi.org/10.1016/j.jas.2011.02.002

Lasaponara, R., and N. Masini, 2012. Image enhancement, feature extraction and geospatial analysis in an archaeological perspective. *Remote Sensing and Digital Image Processing*, 16, 17–47. https://doi.org/10.1007/978-90-481-8801-7_2

Lillesand, T. M., Kiefer, R. W., and J.W. Chipman, 2015. *Remote sensing and image interpretation: seventh edition*. Hoboken: Wiley. ISBN 978-1-118-34328-9

Malakasioti, Z., 2004. The Excavated Burial Mounds in the Voulokaliva Area, in H.R. Reinders (ed.), *Prehistoric Sites at the Almirós and Soúrpi Plains (Thessaly, Greece).* Assen: Koninklijke Van Gorcum, 114-115.

McLeester, M., Casana, J., Schurr, M.R., Hill, A.C., and J.H. Wheeler, 2018. Detecting prehistoric landscape features using thermal, multispectral, and historical imagery analysis at Midewin National Tallgrass Prairie, Illinois. *Journal of Archaeological Science: Reports 21*, 450–459. https://doi.org/10.1016/j.jasrep.2018.08.016

Musson, C., Palmer, R., and S. Campana, 2013. Flights into the Past. Aerial photography, photo interpretation and mapping for archaeology (Issue 4). https://doi.org/10.11588/propylaeumdok.00002009.

Pix4D, 2019. *About Pix4d Mapper.* https://www.pix4d.com/product/pix4dmapperphotogrammetry-software, accessed on 2 April 2021

Perisset, M. C., and A. Tabbagh, 1981. Interpretation of Thermal Prospection on Bare Soils. *Archaeometry*, 23(2), 169–187. https://doi.org/10.1111/j.1475-4754.1981.tb00304.x

Rączkowski, W., 2014. Aerial Archaeology, in C. Smith (eds), *Encyclopedia of Global Archaeology*. New York: Springer. https://doi.org/10.1007/978-1-4419-0465-2_1504

Reinders, H.R., Efstathiou, A., and Z. Malakasioti, 1991. Een survey in het gebied ten noorden van Hellenistisch Halos (Griekenland). *Paleo-Aktueel 2*, 82–86.

Reinders, H.R., Floras, S., Karimali, E., Malakasioti, Z., Prummel, W., Rondiri, V., Sgouras, I. and M. Wijnen, 1997. Karatsádaghli. A Neolithic site in the Almirós plain (Thessaly, Greece). *Pharos: Journal of the Netherlands Institute in Athens* 5, 85–143.

Renfrew, C., and P. Bahn, 2016. *Archaeology: Theories, Methods, and Practice (Seventh Edition).* London: Thames & Hudson.

Reinders, H.R., 2004. *Prehistoric Sites at the Almirós and Soúrpi Plains (Thessaly, Greece).* Assen: Koninklijke Van Gorcum.

Reinders, H.R., 2014. *The city of New Halos and its southeast gate*. Groningen: Barkhuis Publishing and University of Groningen Library.

Rehren, T., Asderaki-Tzoumerkioti, E., and Z. Malakasioti, 2006. The Geometric Tomb at the Site of Voulokaliva: A First Archaeometric Approach, in A. Mazarakis-Ainain (eds.), *Proceedings of the Conference "To archaeologiko Ergo ste Thessalia kai Sterea Ellada" (Volos, March 16-19, 2006), Volume I*. Volos: University of Thessaly, 207–216.

Risbøl, O. and L. Gustavsen, 2018. LiDAR from drones employed for mapping archaeology – Potential, benefits and challenges. *Archaeological Prospection* 25(4), 329–338. https://doi.org/10.1002/arp.1712

Salgado Carmona, J. Á., Quirós, E., Mayoral, V., and C. Charro, 2020. Assessing the potential of multispectral and thermal UAV imagery from archaeological sites. A case study from the Iron Age hillfort of Villasviejas del Tamuja (Cáceres, Spain). *Journal of Archaeological Science: Reports* 31. https://doi.org/10.1016/j.jasrep.2020.102312

Sarris, A., (ed.) 2015. *Best practices of geoinformatic technologies for the mapping of archaeolandscapes*. Oxford: Archeopress. ISBN: 9781784911621.

Stissi, V., 2004. Early Iron Age, in H.R. Reinders (ed.), *Prehistoric Sites at the Almirós and Soúrpi Plains (Thessaly, Greece).* Assen: Koninklijke Van Gorcum, 94-113.

Stissi, V.V., 2011. Finding the Early Iron Age in field survey: Two case studies from Boeotia and Magnesia, In S. Verdan, T. Theurillat, and A.K. Pfyffer (eds.), *Proceedings of the International Round Table organized by the Swiss School of Archaeology in Greece (Athens, November 28–30, 2008)*, 149–162.

Stissi, V.V., Heymans, E., Dijkstra, T., Reinders, H.R., Agnousiotis, D., Efstathiou, D., Kamphorst, S., Mamloudi, I., Rondiri, V., Van Rookhuijzen, J., and E. Stamelou, 2015a. Halos: Preliminary Report of the 2013-2014 Trial Trenches at Magoula Plataniotiki. *Pharos: Journal of the Netherlands Institute in Athens* 21(2), 85–116. https://doi.org/10.2143/PHA.21.2.3206296

Stissi, V.V., Waagen, J., Efstathiou, D., Reinders, H.R., Rondiri, V., Mamloudi, I. and E. Stamelou, 2015b. Halos: Preliminary Report of the 2011-2013 Field Survey Campaigns. *Pharos: Journal of the Netherlands Institute in Athens* 21(2), 63–84. https://doi.org/10.2143/PHA.21.2.3206295

Toth, C., and G. Jóźków, 2016. Remote sensing platforms and sensors: A survey. *ISPRS Journal of Photogrammetry and Remote Sensing* 115. 22–36. https://doi.org/10.1016/j.isprsjprs.2015.10.004

Tsiouka, F., 2008. *Νεκροταφείο της Πρώιμης Εποχής του Σιδήρου στη θέση « Βουλοκαλύβα » (Αρχαία Άλος)*. (Master's thesis. University of Thessaly, Volos, Greece).

Verhoeven, G., 2017. The reflection of two fields – Electromagnetic radiation and its role in (aerial) imaging. *AARGnews*, 55. 13-18. http://doi.org/10.5281/zenodo.3534245

Wace, A.J.B. and M.S. Thompson, 1911-1912. Excavations at Halos. *BSA* 18, 1-29.

Wijnen, M. and V. Neolithic , in H.R. Reinders (ed.), *Prehistoric Sites at the Almirós and Soúrpi Plains (Thessaly, Greece).* Assen: Koninklijke Van Gorcum, 20-38.

List of figures, tables, appendices

Figures

Figure 4.5: An overview of the features on site C. Shown are the optical orthoimage and thermogram of the flight of 06:00 a.m. on the 10th of July (own work).

Figure 4.6: Side-by side view of the optical ortho-image and the thermogram showing a concentration of surface artefacts on site C's Mound 48 (own work).

Figure 4.7: Side-by-side view of the optical ortho-image, thermogram, and digital elevation model for Mound 5 on site C (own work).

Figure 4.8: A comparison of several thermograms of the same area across surveys at 100m altitude (own work).

Figure 4.9: An overview of the mounds at both site B and site C (own work).

Figure 4.10: Two examples of difference maps of site B (own work).

Figure 4.11: The standard deviation map of site, and the first three principal components of site B visualized as an RGB composite (own work).

Figure 4.12: This detail of the possible mound 44 on site B shows the Local Dominance overlaid with the thermal data using the 'lighten' blend method (own work).

Tables

Table 1: A summary of expected archaeological features at the site of Halos and their hypothesised signal on the thermal images.

Table 2: Overview of the analysed flights, with associated environmental variables and GSD.

Table 3: A summary of expected archaeological features at the site of Halos and their hypothesised signal on the thermal images, contrasted with thermal anomalies discovered in the field.

Appendices

Appendix 1: A chronology of the Halos area along with associated sites for each period (based on the chronology proposed in Reinders 2004, 5).

Appendix 2: Thermograms of site B.

Appendix 3: Thermograms of site C.

Period	(Sub)period	Dating	Karatsádagli	Magoúla Zerélia	Pirasos	Voulokaliva 1990/35	Voulokaliva funerary landscape	Magoúla Plataniotiki	Voulokaliva 1990/14	New Halos	Almiros /Armiro	Ayios Nikolaos
Neolithic	Early Neolithic	6700/6500 - 5800/5600 BCE	■		■							
	Middle Neolithic	5800/5600 - 5400/5300 BCE	■	■	■							
	Late Neolithic	5400/5300 - 4700/4500 BCE		■		■						
	Final Neolithic	4700/4500 - 3300/3100 BCE		■		■						
Bronze Age	Early Bronze Age	3300/3100 - 2300/2200 BCE		■		■						
	Middle Bronze Age	2300/2200 - 1700/1500 BCE		■		■		■				
	Late Bronze Age	1700/1500 - 1100/1050 BCE		■		■		■				
Early Iron Age	Protogeometric	1075/1050 - 700/650 BCE				■	■	■				
	Sub-Protogeometric	1050 - 900/850 (?) BCE				■	■	■				
	Geometric	900/850 - 800/750 (?) BCE				■	■	■				
	Late Geometric	750 - 700/680 BCE				■	■	■				
	Sub-Geometric	700/680 - 650/600 (?) BCE					■	■				
Archaic		675/650 - 600/480 BCE					■	■	■			
Classical		480 - 323 BCE		■			■	■				
Hellenistic		323 - 146 BCE		■			■	■			■	
Roman		146 BCE - 324 CE										
Byzantine		324 - 1453 CE				■				■	■	
Ottoman		1453 - 1821 CE				■						■

Appendix 1: A chronology of the Halos area along with associated sites for each period (based on the chronology proposed in Reinders 2004, 5).
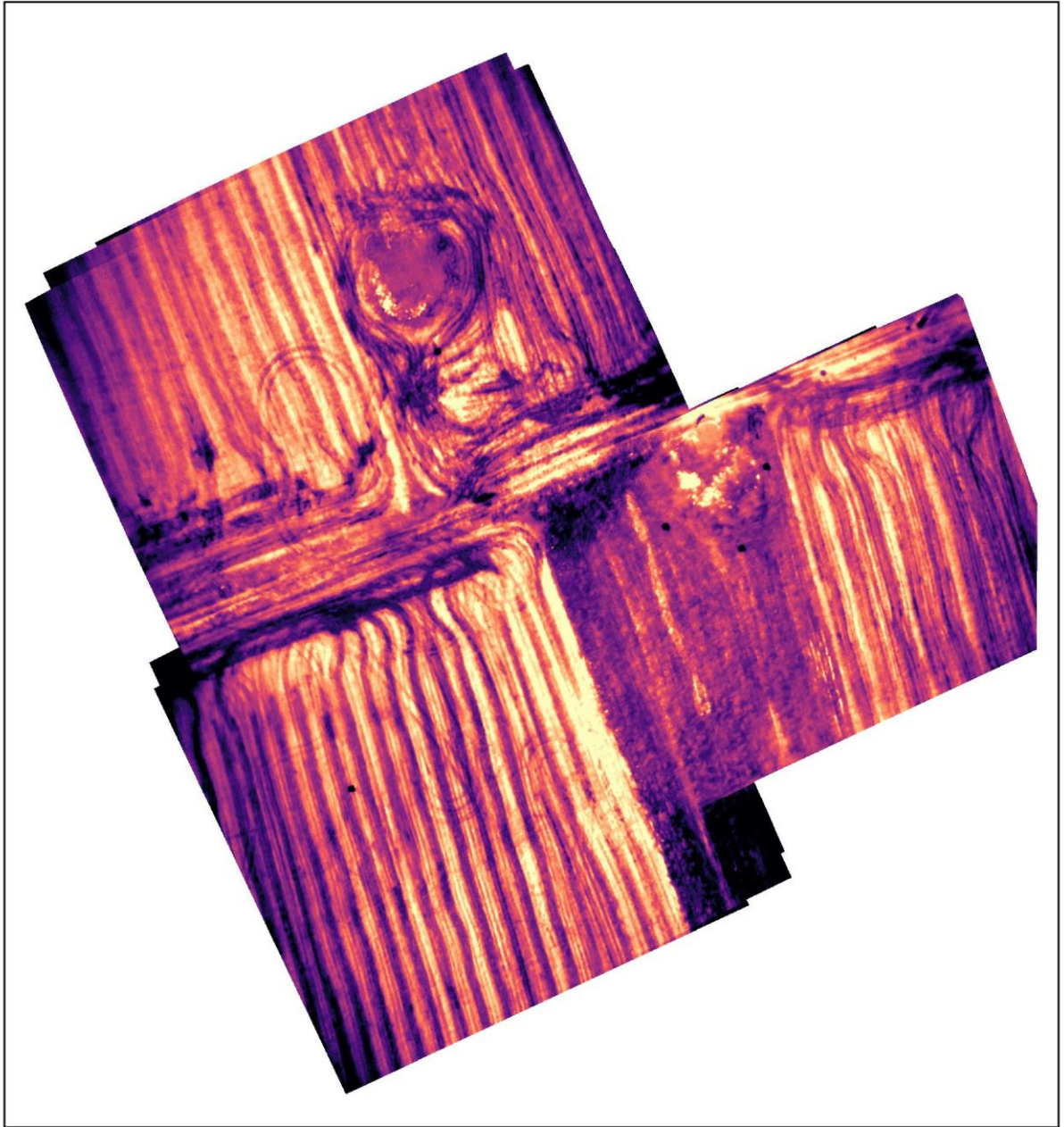
Appendix 2: Thermograms of site B
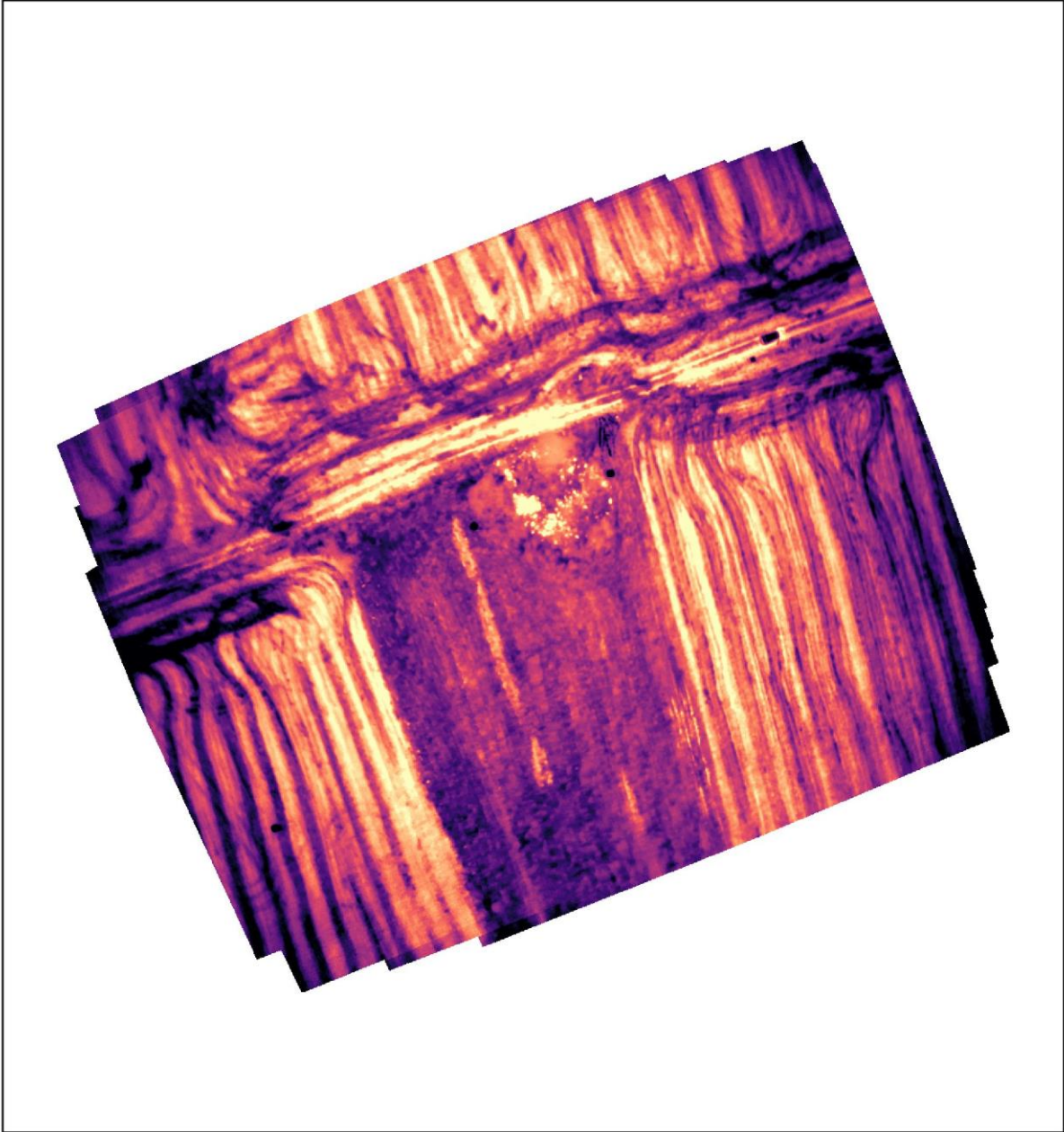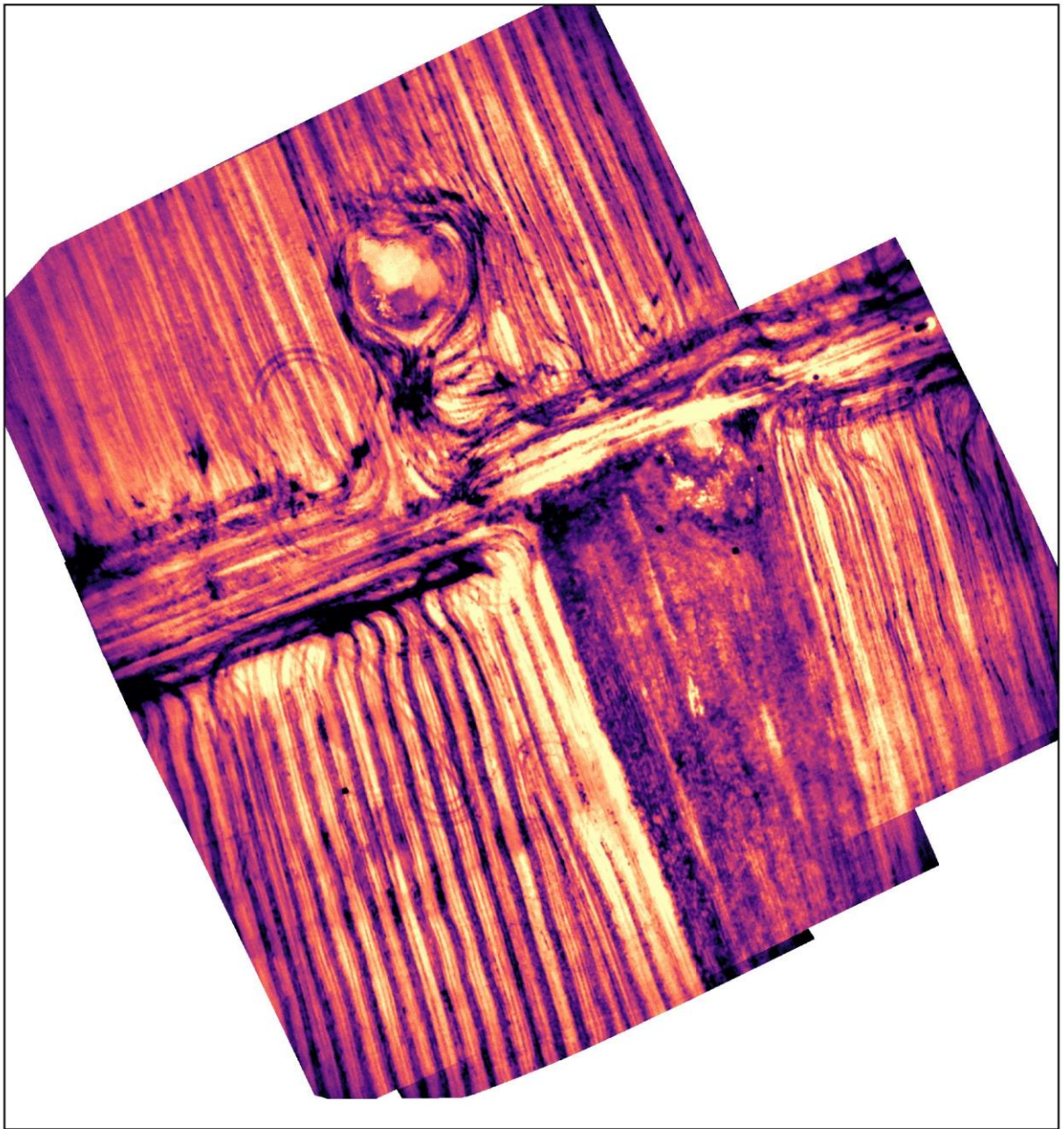

0　10　20　30 m

Thermogram
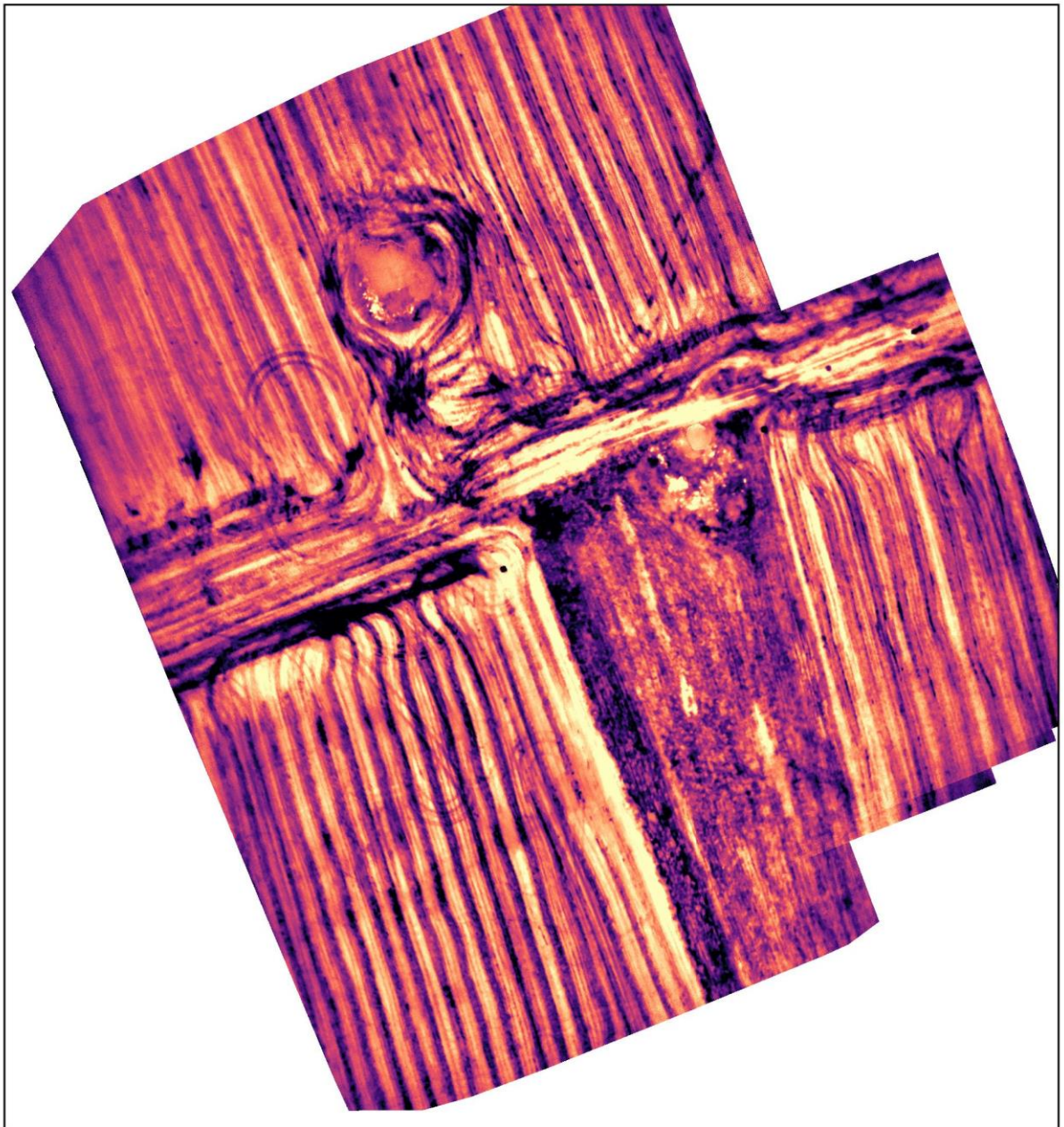20:55, 06-07-2019
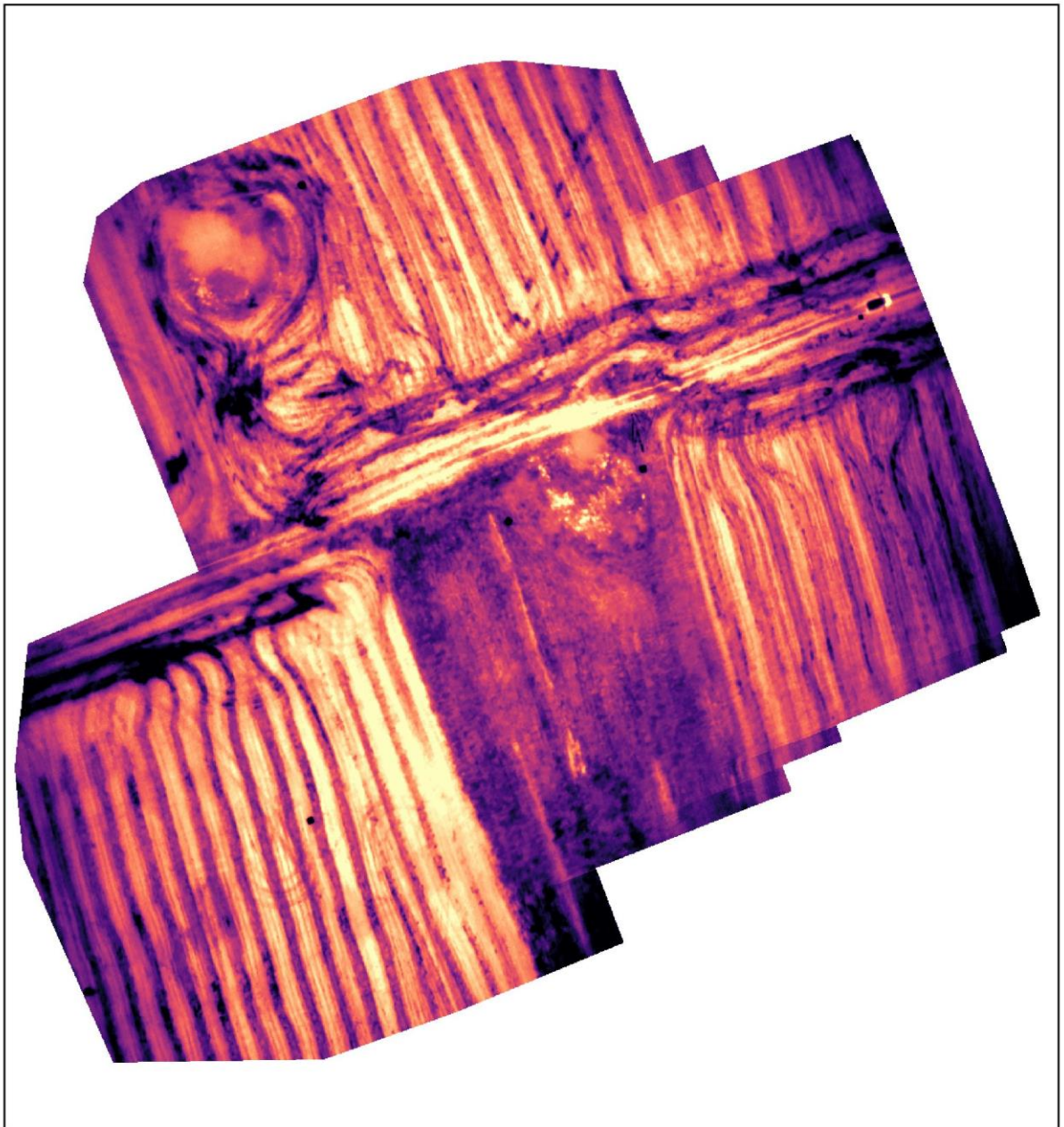
0 10 20 30 m

Thermogram
05:23, 07-07-2019
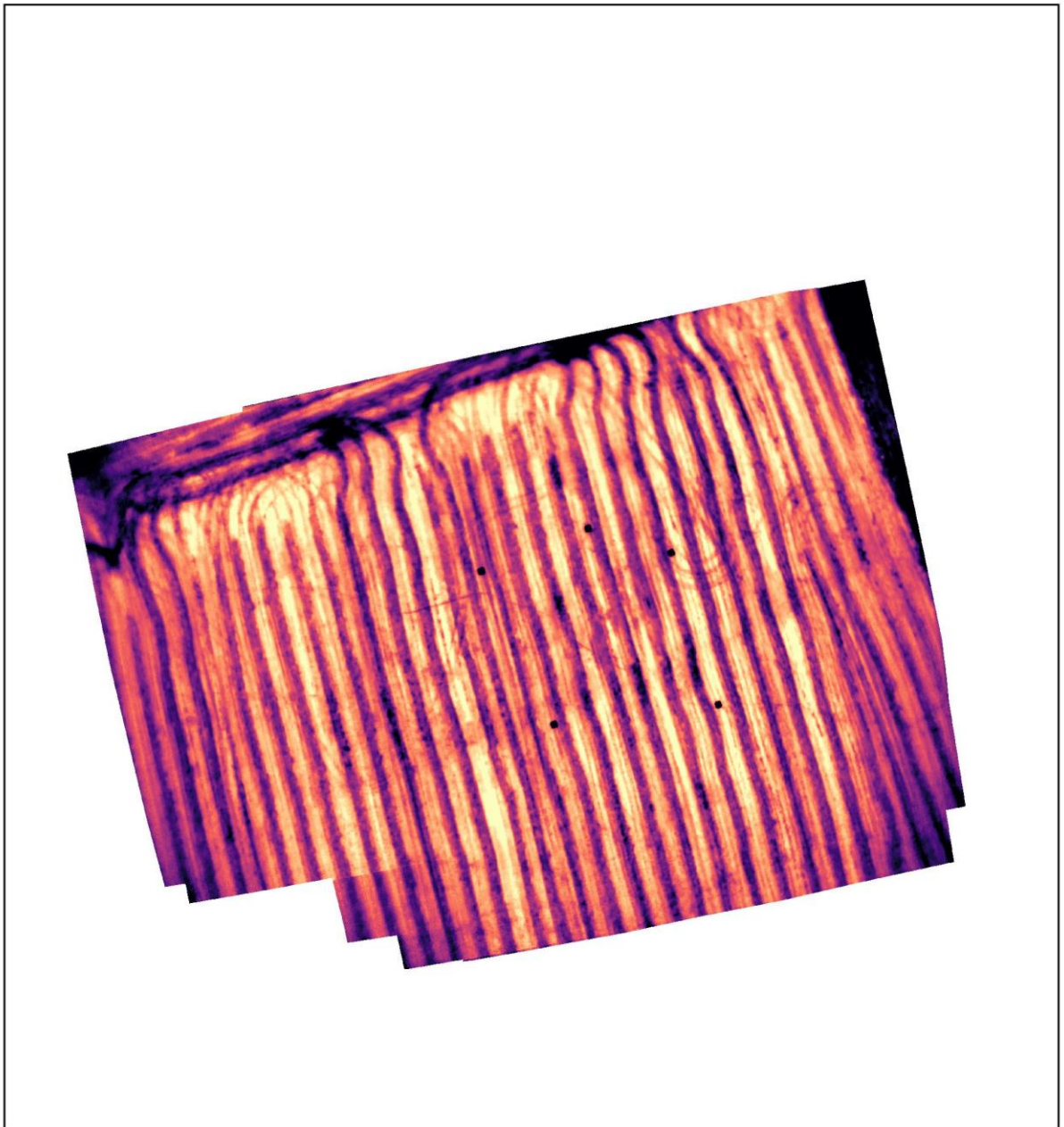
0   15   30   45 m

Thermogram
19:58, 07-07-2019

0   15   30   45 m

Thermogram
06:24, 08-07-2019

Thermogram
01:36, 09-07-2019

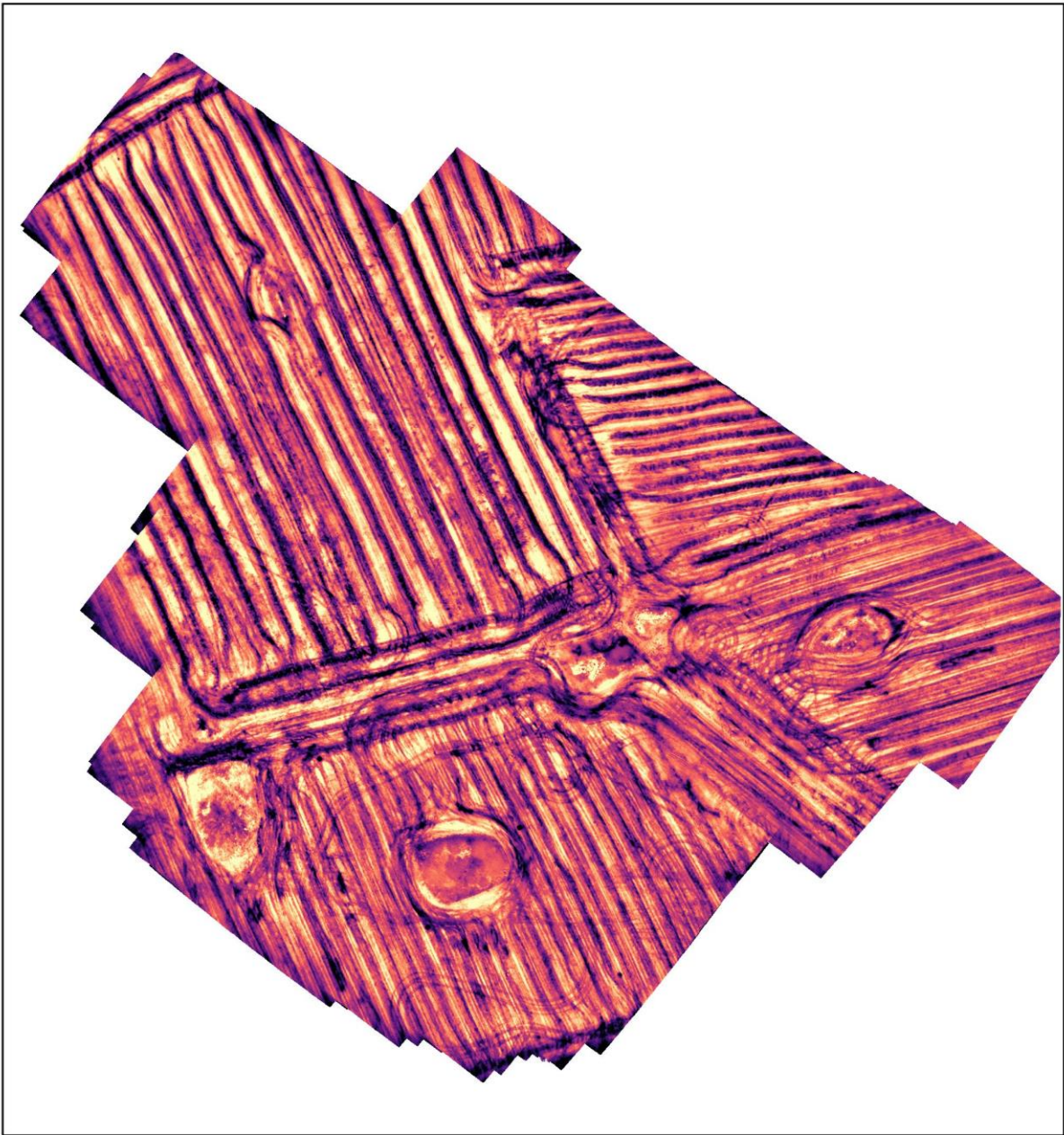0   15   30   45 m

0 10 20 30 m

Thermogram
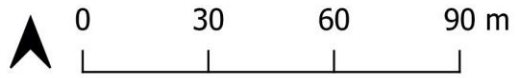20:58, 09-07-2019

0   10   20   30 m

Thermogram
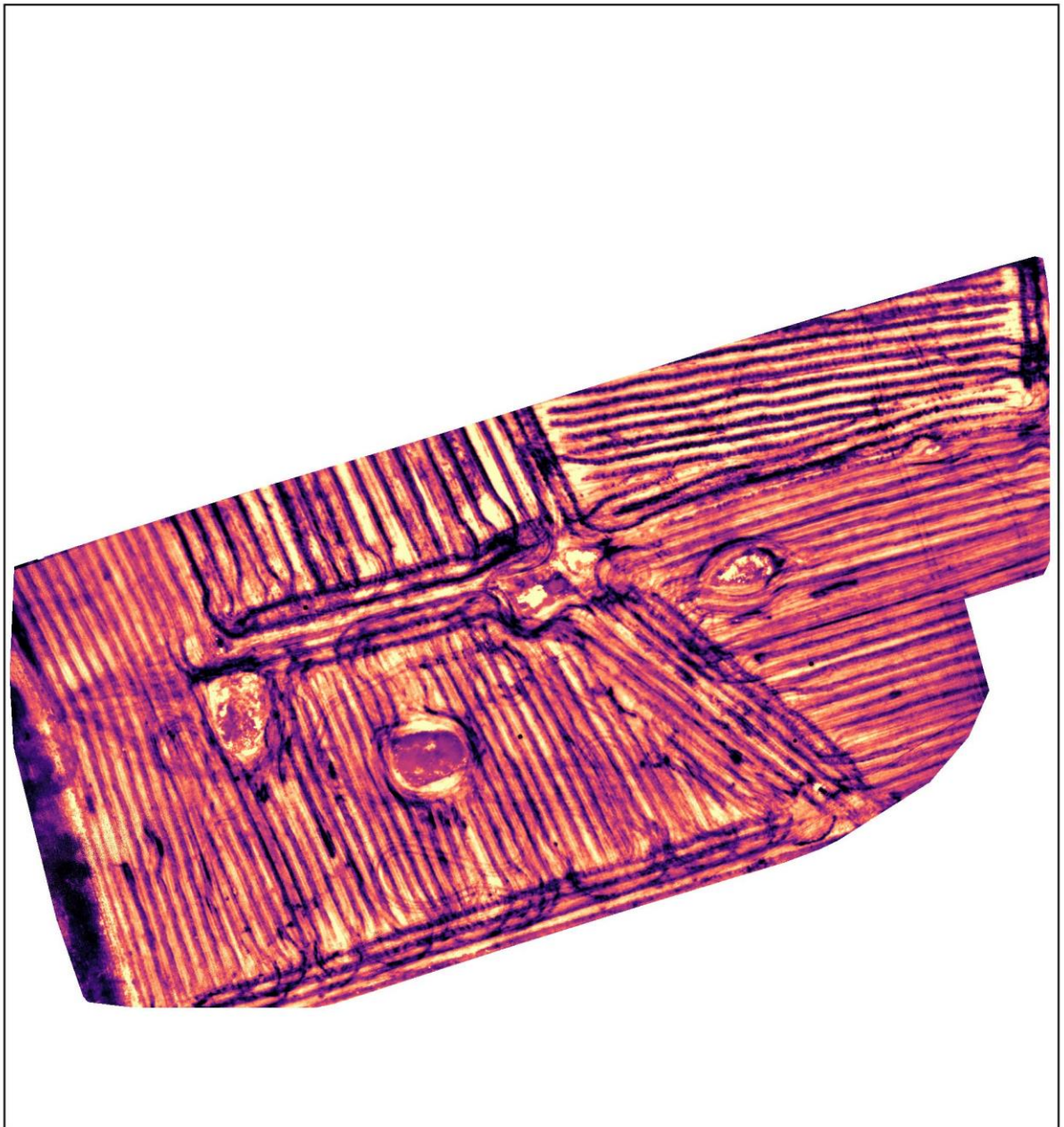05:35, 10-07-2019

Appendix 3: Thermograms of site C

0   15   30   45 m

Thermogram
06:00, 10-07-2019

0   30   60   90 m

Thermogram
21:24, 10-07-2019